SAFETY IMPLICATIONS OF A SENSITIVITY ANALYSIS OF THE REACTOR KINETICS PARAMETERS FOR FAST BREEDER REACTORS

by

Robert Joseph Florian

Dissertation submitted to the Faculty of the
Virginia Polytechnic Institute and State University
in partial fulfillment of the requirements for the degree of

DOCTOR OF PHILOSOPHY

in

Nuclear Science and Engineering

APPROVED:

Ronald J. Onega, Chairman

Milton C. Edlund

Thomas F. Parkinson

James R. Thomas

Robert L. Whitelaw

September, 1982

Blacksburg, Virginia

TABLE OF CONTENTS

TABLE OF CONTENTS
(continued)

ACKNOWLEDGEMENTS

Special thanks go to Dr. Ronald J. Onega for serving as my committee chairman and for his guidance during the course of this research project. Thanks also go to Drs. M. C. Edlund, J. R. Thomas, T. F. Parkinson, and R. L. Whitelaw for serving on my committee and for their encouragement.

I would like to thank my family for all the loving support they have given me during my graduate studies.

I would also like to thank my room-mate, John "Animal" Menna, for putting up with my Aussie ways; Mark J. Embrechts, for his constant encouragement over the past few years; and my favourite beer-drinking mate, Mark Eckenrode, who can down Foster's lager almost as fast as I can.

Last, but not least, I would like to thank Mrs. Neta Byerly for the meticulous manner in which she typed this manuscript.

LIST OF FIGURES

LIST OF TABLES

LIST OF TABLES
(continued)

Chapter 1

INTRODUCTION

1.1 Statement of Problem - Background and Importance

In light of the ever-growing energy problems in both the USA and the rest of the world, there is little doubt that the need for safe and efficient nuclear power will continue for many years to come. However, with several new nuclear plants projected to come on line each year for the next decade [1], one must raise the question of assured uranium resources. There will undoubtedly be a heavy burden on our resources. In order to alleviate this problem, the current administration is planning to pursue a vigorous breeder reactor development programme [2].

Many technical problems remain to be solved before the breeder reactor may be commercially deployed in the USA. One particular class of problems, known as reactor kinetics and dynamics problems, which are essential in reactor safety design [3], rely very much on experimentally determined parameters referred to as kinetics parameters. The parameters of particular interest in this study are the spectra of delayed neutrons. These are important for fast breeder dynamics and safety calculations.

If the kinetics parameters are known, then, from the solutions of the reactor kinetics equations [4] predictions of the transient responce of a reactor, either under normal operating or accident conditions, can be made. During a reactor transient, some of the kinetics parameters may change. By varying the values of the parameters in a transient calculation, the resulting variation in the transient responce may be

predicted. This type of an analysis is referred to as "sensitivity analysis", i.e., the analysis of variations in the responce with respect to variations in the parameters.

In this work, sensitivity will be used in a slightly different sense. The variations in the parameters will be uncertainties, hence the resulting variation in the responce will be the uncertainty in the responce. The parameters of interest are the spectra of the delayed neutrons.

Saphier et. al. [5] have shown that variations in the delayed neutron spectra have a significant effect on the results of dynamic fast reactor transient calculations. This indicates the need for the precise determination of delayed neutron data.

Some of the most recent work in this field has been performed by Reeder and Warner [6]. They have compiled average energies and delayed neutron spectra for 34 precursors from the literature to give a set of best values. Average energies and spectra were calculated for six delayed neutron groups. The bases for their work were two sets of spectral data: one set by Shalev and Rudstam at the OSIRIS separator at Studsvik, Sweden; the other by Kratz of the University of Mainz.

Reeder and Warner calculated one-parameter Maxwellian energy distributions and compared these with the precursor spectra obtained by the above mentioned workers. The one parameter was the average energy of the individual spectra. In several cases, they found that the Maxwellian distribution compared well with the spectra obtained by the Mainz group, although it lacked in fine-group structure. Conflicting results were obtained when compared with the Studsvik spectra. The conflict occurred

in the low energy range (< 50 KeV). This is due to the lack of experimental data in the low energy region. The Studsvik group used a semi-empirical extrapolation of the spectra in this range which resulted in a peak in the spectra below 50 KeV in many cases. The agreement with the Maxwellian distribution is even worse at low energies for fast-neutron-induced fission.

Reeder and Warner [6] have stated, "The present state of ambiguity gives experimentalists some incentive for studying this region of the delayed neutron spectra with greater accuracy" [6].

This state of ambiguity was also the incentive for the work in this dissertation. A sensitivity analysis is performed to determine the sensitivity of a reactor's responce, during a transient, to variations in the delayed neutron spectra which appear explicitly in the reactor kinetics equations.

1.2 Literature Review

Most of the work done on sensitivity analysis has been based on perturbational and variational methods [7]. This section contains a survey of some recent literature in the field of sensitivity analysis. It gives an indication of the reasons for choosing the sensitivity methodology employed in this work.

Recently, a sensitivity methodology was developed by Oblow [8]. He defined the target responce as an integral functional with the integrand being a function of the dependent variable of the system and also a function of the system parameters (or data field). If a small increment

is added to the parameters, a new responce may be written as a Taylor expansion of the increment. From the expansion, an expression for the variation in the responce may be obtained. If a first-order approximation is made, the task is then to find the derivative of the responce with respect to the parameter.

Dubi and Dudziak [9] found this approach to be questionable. They pointed out a number of problems with Oblow's approach; he did not give a clear meaning of the derivative of the responce with respect to the parameters, there were dimensional inconsistencies in his analysis, and the assumed form of the Taylor expansion was given without proof. Dubi and Dudziak presented an alternate differential approach to sensitivity analysis which leads to explicit expressions for the first-order perturbation as well as any higher-order terms by interpretting the differential terms as being Fréchet derivatives. This is necessary because the responce may be a functional, whose domain is a set of functions, so differentiation in the ordinary sense does not apply. The concept of the Fréchet derivative is discussed in Appendix 1.

Cacuci et. al. [10] developed a generalised sensitivity theory for general systems of coupled nonlinear operator equations with nonlinear responces. It is a mathematically rigorous formalism based on the use of adjoint functions. They have unified the differential and variational approaches to sensitivity analysis and showed that they lead to identical sensitivity expressions. The unifying concept is the concept of the Fréchet derivative.

The major motivation behind the work presented in this dissertation was stimulated by the need to study the sensitivity of liquid-metal fast

breeder reactor (LMFBR) transient calculations with respect to the uncertainties in the delayed neutron spectra. With the advent of Cacuci's theory, such a sensitivity analysis can be put on a rigorous mathematical basis. The work presented here will also provide an additional test of his theory for a different class of problems, namely, a system of coupled linear operator equations with linear responces.

Chapter 2

THEORETICAL DEVELOPMENT

2.1 Concept of Sensitivity

Perhaps the simplest way to introduce the concept of sensitivity is by way of an example. The following example was taken from Tomovic [11].

Consider the dependence of the solutions of a system of linear algebraic equations on disturbances of the coefficients. In matrix form, the system is

$$\underline{\underline{A}}\ \underline{x} = \underline{B} \ . \tag{2.1.1}$$

The "disturbed" system is

$$(\underline{\underline{A}} + \Delta\underline{\underline{A}})\ (\underline{x} + \Delta\underline{x}) = \underline{B} \ , \tag{2.1.2}$$

where $\Delta\underline{x}$, the disturbance in $\underline{x}$, is due to $\Delta\underline{\underline{A}}$, the disturbance in $\underline{\underline{A}}$. Subtracting equation (2.1.1) from (2.1.2) and neglecting higher order terms, the following equation is obtained for computing $\Delta\underline{x}$:

$$\underline{\underline{A}}\ \Delta\underline{x} + \Delta\underline{\underline{A}}\ \underline{x} = 0 \ .$$

Substituting for $\underline{x}$ leads to

$$\Delta\underline{x} = -\underline{\underline{A}}^{-1}\ \ \Delta\underline{\underline{A}}\ \underline{\underline{A}}^{-1}\ \underline{B} \ . \tag{2.1.3}$$

Alternatively, the following method can be used to achieve the same result. For simplicity, consider a system of two linear algebraic equations:

$$a_{11}\ x_1 + a_{12}\ x_2 = b_1, \text{ and}$$

$$a_{21}\, x_1 + a_{22}\, x_2 = b_2 \ .$$

Suppose the disturbances in the solution are due to a_{11}. The sensitivity derivatives can be defined as

$$\frac{\partial x_1}{\partial a_{11}} = u_1 \quad \text{and} \quad \frac{\partial x_2}{\partial a_{11}} = u_2 \ .$$

By differentiating the above system of equations with respect to a_{11}, and using the definitions of the sensitivity derivatives, the following system of equations for the sensitivity derivatives is obtained:

$$a_{11}\, u_1 + a_{12}\, u_2 = -x_1 \ , \text{ and}$$

$$a_{21}\, u_1 + a_{22}\, u_2 = 0 \ .$$

Similarly, the sensitivity derivatives with respect to a_{22},

$$\frac{\partial x_1}{\partial a_{22}} = \nu_1 \text{ and } \frac{\partial x_2}{\partial a_{22}} = \nu_2 \ ,$$

give rise to the equations

$$a_{11}\, \nu_1 + a_{12}\, \nu_2 = 0 \ , \text{ and}$$

$$a_{21}\, \nu_1 + a_{22}\, \nu_2 = - x_2 \ .$$

Since the system of equations (2.1.1) is linear, simultaneous disturbances of more than one parameter are obtained by the principle of superposition:

$$\Delta \underline{x} = \begin{bmatrix} u_1 \\ u_2 \end{bmatrix} \Delta a_{11} + \begin{bmatrix} \nu_1 \\ \nu_2 \end{bmatrix} \Delta a_{22} \ .$$

When studying dynamic systems, it is of interest to know the sensitivity of a system responce with respect to changes in the system parameters. The system responce may be the dependent variables of the system (solutions of the governing equations), or it may be some combination of the dependent variables.

If the responce is represented by R, and the system parameters by the vector $\underline{\alpha} = (\alpha_1, \alpha_2, \ldots, \alpha_l)$, then the main task in the sensitivity analysis is to derive the set of sensitivity derivatives

$$\frac{dR}{d\alpha_i} ,$$

from which the variation in the responce due to variations in the parameters may be found by

$$\delta R = \sum_{i=1}^{l} \frac{dR}{d\alpha_i} \delta\alpha_i .$$

The purpose of a sensitivity analysis may be two-fold. Firstly, the values of the parameters may be well-known. One may simply be interested in how the system responce varies as the parameters vary. Or secondly, the parameters may not be well-known, so one would then be interested in calculating the uncertainty in the system responce with respect to the uncertainties in the parameters.

2.2 General Development

2.2.1 Introduction

The basis of this study is the generalised sensitivity theory developed by Cacuci et. al. [10]. While the theory was developed for general systems of coupled nonlinear equations, it should be equally applicable to systems of linear equations. The sensitivity theory for general systems of nonlinear equations will be described below. The development closely follows that of Cacuci et. al. for the differential approach. In section 2.3, a detailed description of the application of this theory to a linear reactor kinetics problem will be presented.

2.2.2 Problem Definition

Consider a system of K coupled nonlinear equations

$$\underline{N}[\underline{X}(\underline{\rho}), \underline{\alpha}(\underline{\rho})] = Q(\underline{\rho},\underline{\alpha}) \ , \tag{2.2.1}$$

where

$$\underline{X}(\underline{\rho}) = [X_1(\underline{\rho}), \ \ldots \ , X_K(\underline{\rho})] \tag{2.2.2}$$

is the state-vector of the system,

$$\underline{\rho} = (\rho_1, \ \ldots \ , \rho_J) \tag{2.2.3}$$

is the phase-space position vector,

$$\underline{Q} = [Q_1(\underline{\rho},\underline{\alpha}), \ \ldots \ , Q_K(\underline{\rho},\underline{\alpha})] \tag{2.2.4}$$

is the inhomogeneous source vector, and

$$\underline{\alpha}(\underline{\rho}) = [\alpha_1(\underline{\rho}), \ \ldots \ , \alpha_I(\underline{\rho})] \tag{2.2.5}$$

is the vector of system parameters (or data field).

(Note: Even though the vectors are written horizontally, they represent column vectors.)

The K components, N_k, of $\underline{N}$, may be differential, difference, or integral operators which may be nonlinear not only in $\underline{X}$ but also in $\underline{\alpha}$.

If equations (2.2.1) contain differential operators, then an appropriate set of boundary conditions must be specified:

$$\underline{B}[\underline{X}(\underline{\rho}^S), \underline{\alpha}] = 0 , \tag{2.2.6}$$

where $\underline{\rho}^S$ denotes a point of the appropriate surface in the phase-space.

2.2.3 Responce Functional

Consider a responce functional represented by

$$R[\underline{X},\underline{\alpha}] = \int_{\underline{\rho}} F[\underline{X}(\underline{\rho}), \underline{\alpha}(\underline{\rho}),\underline{\rho}] \, d\underline{\rho} , \tag{2.2.7}$$

where F is in general a function of $\underline{X}$ and $\underline{\alpha}$. The goal of the sensitivity theory is to derive expressions for the sensitivity derivatives $dR/d\alpha_i$. "These quantities can be used not only to estimate the changes in R due to changes in α_i, but also to rank the relative importance of input data and to calculate uncertainties in R due to uncertainties in the parameters"[10].

2.2.4 Differential Approach to Sensitivity Analysis

To find the variation in the responce functional, take the Fréchet differential of equation (2.2.7):

$$\delta R = \int_{\underline{\rho}} F'_{\underline{X}} \, \delta \underline{X}(\underline{\rho}) d\underline{\rho} + \int_{\underline{\rho}} F'_{\underline{\alpha}} \, \delta \underline{\alpha}(\underline{\rho}) d\underline{\rho}$$

$$= \delta R_{\underline{X}} + \delta R_{\underline{\alpha}} \, , \qquad (2.2.8)$$

"where $F'_{\underline{X}} = (F'_{X_1}, \ldots, F'_{X_K})$ and $F'_{\underline{\alpha}} = (F'_{\alpha_1}, \ldots, F'_{\alpha_I})$ are vectors whose components represent Fréchet derivatives of F with respect to the functions X_k and α_i respectively" [10]. An implicit assumption throughout this work will be that Fréchet derivatives exist wherever needed. The first term, $\delta R_{\underline{X}}$, in equation (2.2.8) is referred to as the indirect effect, while the second term, $\delta R_{\underline{\alpha}}$, is referred to as the direct effect.

$\delta \underline{X}$ must be determined in order to evaluate equation (2.2.8). A system of equations for $\delta \underline{X}$ may be obtained by taking the Fréchet differentials of equations (2.2.1) and (2.2.6), giving

$$\underline{\underline{L}} \delta \underline{X} = \underline{\underline{S}} \delta \underline{\alpha} \, , \text{ and} \qquad (2.2.9)$$

$$\underline{B}'_{\underline{X}} \, \delta \underline{X} = - \underline{B}'_{\underline{\alpha}} \, \delta \underline{\alpha} \, , \qquad (2.2.10)$$

where $\underline{\underline{L}}$ and $\underline{\underline{S}}$ are matrices defined as

$$L_{kr} \equiv (N_k)'_{X_r} \, , \; k = 1, \ldots, K; \; r = 1, \ldots, K; \text{ and}$$

$$S_{ki} \equiv (Q_k)'_{\alpha_i} - (N_k)'_{\alpha_i} \, , \; k = 1, \ldots, K; \; i = 1, \ldots, I.$$

In words, $\underline{\underline{L}}$ is the Fréchet derivative of $\underline{N}$ with respect to $\underline{X}$, and $\underline{\underline{S}}$ is the Fréchet derivative of $\underline{Q} - \underline{N}$ with respect to $\underline{\alpha}$.

It should be noted, at this point, that equations (2.2.9) and (2.2.10) contain sufficient information to calculate $\delta \underline{X}$, and hence δR, for any change $\delta \underline{\alpha}$. However, if a large number of changes are to be analysed, this could become a mammoth task.

The existence of the Fréchet derivatives guarantees that equations (2.2.9) and (2.2.10) are linear in $\delta\underline{X}$, hence, an alternate approach based on adjoints will be used. An operator $\underline{\underline{L}}^*$, adjoint to $\underline{\underline{L}}$, may be defined by

$$<\underline{\underline{L}}^* \underline{\Phi}, \delta\underline{X}> = <\underline{\Phi}, \underline{\underline{L}}\delta\underline{X}> + P[\underline{\Phi},\delta\underline{X}] \ , \tag{2.2.11}$$

where $\underline{\Phi} = (\Phi_1 \ \ldots \ , \Phi_K)$ is the vector adjoint to $\delta\underline{X}$ and $P[\underline{\Phi}, \delta\underline{X}]$ is the bilinear concomitant of $\underline{\Phi}$ and $\delta\underline{X}$ evaluated on the appropriate boundary in the phase-space. The inner products in equation (2.2.11) are defined by

$$<\underline{\Phi}, \underline{\Psi}> \equiv \int_{\underline{\rho}} \underline{\Phi} \cdot \underline{\Psi} d\underline{\rho} \ . \tag{2.2.12}$$

The system of equations adjoint to equations (2.2.9) may be written as

$$\underline{\underline{L}}^* \underline{\Phi} = \underline{\$}^* \ , \tag{2.2.13}$$

where the adjoint operator $\underline{\underline{L}}^*$ is found by application of equation (2.2.11) giving

$$\underline{\underline{L}}^* = [L^*_{rk}] \ , \qquad k, r = 1, \ \ldots \ , K \ .$$

$\underline{\underline{L}}^*$ is a K X K matrix found by transposing the adjoints of the elements of $\underline{\underline{L}}$.

Also during the application of equation (2.2.11), the appropriate boundary conditions

$$\underline{B}^*[\underline{\Phi}] = 0 \tag{2.2.14}$$

are obtained by " ... requiring that

1. $\underline{B}^*$ be independent of $\delta\underline{\alpha}$, $\delta\underline{X}$ and Fréchet derivatives with respect to $\underline{\alpha}$, and
2. all terms in $P[\underline{\Phi}, \delta\underline{X}]$ that contain unknown values of $\delta\underline{X}$ must vanish." [10]

Condition 2 reduces $P[\underline{\Phi}, \delta\underline{X}]$ to $\hat{P}[\underline{\Phi}, \delta\underline{X}]$ containing only known values of $\delta\underline{X}$ evaluated on the boundary.

Substituting equations (2.2.9) and (2.2.13) into equation (2.2.11) gives

$$<\underline{\$}^*, \delta\underline{X}> = <\underline{\Phi}, \underline{\underline{S}}\delta\underline{\alpha}> + \hat{P}[\underline{\Phi}, \delta\underline{X}] \quad . \tag{2.2.15}$$

Comparing equations (2.2.15) and (2.2.8), and choosing

$$\underline{\$}^* = F'_{\underline{X}} \quad , \tag{2.2.16}$$

equation (2.2.8) becomes

$$\delta R = \delta R_{\underline{\alpha}} + <\underline{\Phi}, \underline{\underline{S}}\delta\underline{\alpha}> + \hat{P}[\underline{\Phi}, \delta\underline{X}] \quad . \tag{2.2.17}$$

"Finally, note that for many practical problems, the components of $\underline{\alpha}$ and $\delta\underline{\alpha}$ are real numbers; hence, $\delta\underline{\alpha}$ can be taken outside of all integrals over $\underline{\rho}$ in the foregoing derivations (assuming $\underline{X}$ sufficiently differentiable). Therefore, in such cases, the equality

$$\delta R = \sum_{i=1}^{I} \frac{dR}{d\alpha_i} \delta\alpha_i \tag{2.2.18}$$

is usually employed. The quantities $dR/d\alpha_i$ are sensitivity derivatives in the usual sense, and can be obtained by eliminating the explicit appearance of $\delta\underline{X}$ and $\delta\underline{\alpha}$ in the foregoing derivations (i.e., employing derivatives instead of differentials). Then, of course, $\underline{\Phi}$ would play the role of an adjoint function to $\partial\underline{X}/\partial\alpha_i$ rather than $\delta\underline{X}$". [10]

Note: Equation (2.2.18) is somewhat misleading. Rather than considering the individual components, α_i, of $\underline{\alpha}$ as parameters, the entire vector $\underline{\alpha}$ should be considered as the parameter. Likewise, the vector $dR/d\underline{\alpha}$ should be considered as the sensitivity derivative of R with respect to the parameter $\underline{\alpha}$.

Then, equation (2.2.18) can be written as a dot product:

$$\delta R = \frac{dR}{d\underline{\alpha}} \cdot \delta\underline{\alpha} \ . \qquad (2.2.19)$$

2.3 Problem Being Studied

2.3.1 Restatement of Problem

The purpose of this work is to study the sensitivity of transient reactor responces to uncertainties in the delayed neutron spectra. For example, it may be of interest to study the effect of these uncertainties on the results of a safety analysis study of a control rod ejection accident. A number of safety related responces will be discussed later.

2.3.2 Description of Reactor

The reactor which will serve as the basis for this study is the reference mixed oxide (MOX) design used in the International Nuclear Fuel Cycle Evaluation (INFCE) fast breeder reactor (FBR) studies [12]. The reactor used in this study is a LMFBR with a MOX core and a radial blanket of depleted uranium. The reactor is rated at 2740 MWt with a net electrical output of 1000 MWe at 36.5% thermal efficiency. The core is controlled by B_4C control rods.

A more detailed description of the core will be given later when the data preparation is discussed.

2.3.3 Theoretical Development

Governing Equations

Before stating the governing equations, the basic assumptions that lead to the particular form of the equations will be listed. Any further assumptions used in regards to the numerical solution of these equations will be discussed later.

The assumptions are:

(1) one-dimensional (radial) spatial model,

(2) two neutron energy groups,

(3) delayed neutrons are produced only by the isotopes U-238 and Pu-239 (two delayed neutron groups per isotope),

(4) the fission spectra in the core and blanket are the same,

(5) no temperature dependence of reactor parameters,

(6) each region in the core is considered homogeneous, hence all the equations contain constant coefficients, and

(7) a quasi static model, commonly called the prompt jump approximation (PJA), is used.

The following development will closely follow the general development presented in section 2.2. References will be made to specific equations in section 2.2.

The governing equations are the reactor kinetics equations. They are

$$D^1\nabla^2\phi^1 - \left[\Sigma_a^1 + \Sigma_p^1 + \Sigma_S^{1/2} + D^1B_z^2\right]\phi^1$$
$$+ \chi_p^1\left\{(1-\beta^8)\left[\nu_8^1\Sigma_{f8}^1\phi^1 + \nu_8^2\Sigma_{f8}^2\phi^2\right] + (1-\beta^9)\left[\nu_9^1\Sigma_{f9}^1\phi^1 + \nu_9^2\Sigma_{f9}^2\phi^2\right]\right.$$
$$\left. + \left[(\nu\Sigma_f)_1^*\phi^1 + (\nu\Sigma_f)_2^*\phi^2\right]\right\}$$
$$+ \lambda_1^8\chi_{1,8}^1C_1^8 + \lambda_2^8\chi_{2,8}^1C_2^8 + \lambda_1^9\chi_{1,9}^1C_1^9 + \lambda_2^9\chi_{2,9}^1C_2^9 = 0 \qquad (2.3.1)$$

for the faster energy group, E ε[0.11 MeV, 10 MeV],

$$D^2\nabla^2\phi^2 - \left[\Sigma_a^2 + \Sigma_p^2 + D^2B_z^2\right]\phi^2 + \Sigma_S^{1/2}\phi^1$$
$$+ \chi_p^2\left\{(1-\beta^8)\left[\nu_8^1\Sigma_{f8}^1\phi^1 + \nu_8^2\Sigma_{f8}^2\phi^2\right] + (1-\beta^9)\left[\nu_9^1\Sigma_{f9}^1\phi^1 + \nu_9^2\Sigma_{f9}^2\phi^2\right]\right.$$
$$\left. + \left[(\nu\Sigma_f)_1^*\phi^1 + (\nu\Sigma_f)_2^*\phi^2\right]\right\}$$
$$+ \lambda_1^8\chi_{1,8}^2C_1^8 + \lambda_2^8\chi_{2,8}^2C_2^8 + \lambda_1^9\chi_{1,9}^2C_1^9 + \lambda_2^9\chi_{2,9}^2C_2^9 = 0 \qquad (2.3.2)$$

for the lower energy group, E $\varepsilon[10^{-5}$eV, 0.11 MeV], and the precursor equations are

$$\beta_1^8\left[\nu_8^1\Sigma_{f8}^1\phi^1 + \nu_8^2\Sigma_{f8}^2\phi^2\right] - \lambda_1^8C_1^8 = \frac{\partial C_1^8}{\partial t}, \qquad (2.3.3)$$

$$\beta_2^8\left[\nu_8^1\Sigma_{f8}^1\phi^1 + \nu_8^2\Sigma_{f8}^2\phi^2\right] - \lambda_2^8C_2^8 = \frac{\partial C_2^8}{\partial t}, \qquad (2.3.4)$$

$$\beta_1^9\left[\nu_9^1\Sigma_{f9}^1\phi^1 + \nu_9^2\Sigma_{f9}^2\phi^2\right] - \lambda_1^9C_1^9 = \frac{\partial C_1^9}{\partial t}, \text{ and} \qquad (2.3.5)$$

$$\beta_2^9\left[\nu_9^1\Sigma_{f9}^1\phi^1 + \nu_9^2\Sigma_{f9}^2\phi^2\right] - \lambda_2^9C_2^9 = \frac{\partial C_2^9}{\partial t}, \qquad (2.3.6)$$

where

ϕ^1, ϕ^2 = two group fluxes at (r,t),

C_1^8, C_2^8 = concentrations, at (r,t), of precursor groups 1 and 2 resulting from the fission of U-238,

C_1^9, C_2^9 = concentrations, at (r,t), of precursor groups 1 and 2 resulting from the fission of Pu-239,

λ_1^8, λ_2^8 = decay constants for precursor groups 1 and 2 resulting from the fission of U-238,

λ_1^9, λ_2^9 = decay constants for precursor groups 1 and 2 resulting from the fission of Pu-239,

D^1, D^2 = two-group diffusion coefficients,

Σ_a^1, Σ_a^2 = two-group macroscopic absorption cross sections,

Σ_p^1, Σ_p^2 = two-group macroscopic poison cross sections,

$\Sigma_s^{1/2}$ = macroscopic group transfer cross section,

$\nu_8^1\Sigma_{f8}^1, \nu_8^2\Sigma_{f8}^2$ = two-group macroscopic production cross sections for U-238,

$\nu_9^1\Sigma_{f9}^1, \nu_9^2\Sigma_{f9}^2$ = two-group macroscopic production cross sections for Pu-239,

$(\nu\Sigma_f)_1^*, (\nu\Sigma_f)_2^*$ = two-group macroscopic production cross sections for all other fissionable isotopes,

B_z^2 = transverse geometrical buckling,

χ_p^1, χ_p^2 = two-group prompt neutron spectra,

β_1^8, β_2^8 = U-238 delayed neutron fractions for precursor groups 1 and 2,

β_1^9, β_2^9 = Pu-239 delayed neutron fractions for precursor groups 1 and 2,

β^8 = $\beta_1^8 + \beta_2^8$,

β^9 = $\beta_1^9 + \beta_2^9$, and

$\chi_{i,j}^g$ = spectrum of delayed neutron precursor group i, resulting from the fission of isotope j, producing neutrons in energy group g (i = 1, 2; j = 8,9; g = 1,2).

The system of equations (2.3.1) to (2.3.6) corresponds to the system (2.2.1). However, the above system is linear and homogeneous. The state vector for the kinetics equations is

$$\underline{X} = [\phi^1, \phi^2, C_1^8, C_2^8, C_1^9, C_2^9] , \tag{2.3.7}$$

and the phase-space position vector is

$$(r,t) \tag{2.3.8}$$

where

r = the spatial (radial) coordinate, and

t = the time coordinate.

The parameter vector (data field) is

$$\underline{\alpha} = (\chi_{1,8}^1, \chi_{1,8}^2, \chi_{1,9}^1, \chi_{1,9}^2, \chi_{2,8}^1, \chi_{2,8}^2, \chi_{2,9}^1, \chi_{2,9}^2) . \tag{2.3.9}$$

Equations (2.3.7) to (2.3.9) correspond to equations (2.2.2), (2.2.3), and (2.2.5).

The boundary and initial conditions are

$$\left.\frac{\partial \phi^1}{\partial r}\right|_{r=0} = 0 \; ; \; \phi^1(R,t) = 0 \; ; \; \phi^1(r,0) = \phi_0^1 \tag{2.3.10}$$

$$\left.\frac{\partial \phi^2}{\partial r}\right|_{r=0} = 0 \; ; \; \phi^2(R,t) = 0 \; ; \quad \phi^2(r,0) = \phi_0^2 \; , \tag{2.3.11}$$

$$c_1^8 \; (t = 0) = \frac{\beta_1^8}{\lambda_1^8}\left[\nu_8^1\Sigma_{f8}^1\phi_0^1 + \nu_8^2\Sigma_{f8}^2\phi_0^2\right] \; , \tag{2.3.12}$$

$$c_2^8 \; (t = 0) = \frac{\beta_2^8}{\lambda_2^8}\left[\nu_8^1\Sigma_{f8}^1\phi_0^1 + \nu_8^2\Sigma_{f8}^2\phi_0^2\right] \; , \tag{2.3.13}$$

$$c_1^9 \; (t = 0) = \frac{\beta_1^9}{\lambda_1^9}\left[\nu_9^1\Sigma_{f9}^1\phi_0^1 + \nu_9^2\Sigma_{f9}^2\phi_0^2\right] \; , \text{ and} \tag{2.3.14}$$

$$c_2^9 \; (t = 0) = \frac{\beta_2^9}{\lambda_2^9}\left[\nu_9^1\Sigma_{f9}^1\phi_0^1 + \nu_9^2\Sigma_{f9}^2\phi_0^2\right] \; , \tag{2.3.15}$$

where R is the outer radius of the reactor.

The initial conditions are found by solving the steady-state form of the governing equations. This is done by means of a criticality search [14]. The solution of these equations will be discussed later when the numerics are discussed.

Responce Functionals

The responce functional that will be considered is defined as

$$R[\phi^1, \phi^2, \underline{\alpha}_0] = \int_0^{t_f}\int_0^{R}\left[f(r,t)\phi^1(r,t;\underline{\alpha}_0) + g(r,t)\phi^2(r,t;\underline{\alpha}_0)\right] \cdot 2\pi H \; r\,dr\,dt \; , \tag{2.3.16}$$

where

$r \in [0,R]$,

$t \in [0,t_f]$,

H = height of reactor,

$f(r,t)$, $g(r,t)$ = arbitrary weight functions,

$\phi^1(r,t;\underline{\alpha}_0)$, $\phi^2(r,t;\underline{\alpha}_0)$ = two-group fluxes evaluated using the unperturbed parameter vector $\underline{\alpha}_0$,

and

$2\pi H\, rdrdt$ = differential element of the phase space.

Fréchet Differentiation of Governing Equations

The next step in the derivation of the differential approach to sensitivity analysis is to differentiate the governing equations and the initial and boundary conditions with respect to the parameter vector $\underline{\alpha}$. Instead of using differentials as in equations (2.2.9) and (2.2.10), derivatives will be used. Further, instead of differentiating with respect to the entire parameter vector, differentiation with respect to only one component will be performed. An example of how to perform the (Fréchet) differentiation is given in Appendix 1.

Assuming that only the state vector depends on the parameters $\underline{\alpha}$, taking the Fréchet derivative of the system of equations (2.3.1) to (2.3.6) with respect to $\alpha_i \in \underline{\alpha}$ results in the following system of equations:

The two-group diffusion equations become

$$D^1\nabla^2\psi^1 - \left[\Sigma_a^1 + \Sigma_p^1 + \Sigma_S^{1/2} + D^1B_z^2\right]\psi^1$$

$$+ \chi_p^1\left\{(1 - \beta^8)\left[\nu_8^1\Sigma_{f8}^1\psi^1 + \nu_8^2\Sigma_{f8}^2\psi^2\right] + (1 - \beta^9)\left[\nu_9^1\Sigma_{f9}^1\psi^1 + \nu_9^2\Sigma_{f9}^2\psi^2\right]\right.$$

$$\left. + \left[(\nu\Sigma_f)_1^*\psi^1 + (\nu\Sigma_f)_2^*\psi^2\right]\right\}$$

$$+ \lambda_1^8\chi_{1,8}^1\psi^3 + \lambda_2^8\chi_{2,8}^1\psi^4 + \lambda_1^9\chi_{1,9}^1\psi^5 + \lambda_2^9\chi_{2,9}^1\psi^6$$

$$= -\left[\lambda_1^8\theta_{1,8}^1 c_1^8(\underline{\alpha}_0) + \lambda_2^8\theta_{2,8}^1 c_2^8(\underline{\alpha}_0) + \lambda_1^9\theta_{1,9}^1 c_1^9(\underline{\alpha}_0) + \lambda_2^9\theta_{2,9}^1 c_2^9(\underline{\alpha}_0)\right]$$

(2.3.17)

for the faster group, and

$$D^2\nabla^2\psi^2 - \left[\Sigma_a^2 + \Sigma_P^2 + D^2B_z^2\right]\psi^2 + \Sigma_S^{1/2}\psi^1$$

$$+ \chi_p^2\left\{(1 - \beta^8)\left[\nu_8^1\Sigma_{f8}^1\psi^1 + \nu_8^2\Sigma_{f8}^2\psi^2\right] + (1 - \beta^9)\left[\nu_9^1\Sigma_{f9}^1\psi^1 + \nu_9^2\Sigma_{f9}^2\psi^2\right]\right.$$

$$\left. + \left[(\nu\Sigma_f)_1^*\psi^1 + (\nu\Sigma_f)_2^*\psi^2\right]\right\}$$

$$+ \lambda_1^8\chi_{1,8}^2\psi^3 + \lambda_2^8\chi_{2,8}^2\psi^4 + \lambda_1^9\chi_{1,9}^2\psi^5 + \lambda_2^9\chi_{2,9}^2\psi^6$$

$$= -\left[\lambda_1^8\theta_{1,8}^2 c_1^8(\underline{\alpha}_0) + \lambda_2^8\theta_{2,8}^2 c_2^8(\underline{\alpha}_0) + \lambda_1^9\theta_{1,9}^2 c_1^9(\underline{\alpha}_0) + \lambda_2^9\theta_{2,9}^2 c_2^9(\underline{\alpha}_0)\right]$$

(2.3.18)

for the slower group.

The precursor equations become

$$\frac{\partial \psi^3}{\partial t} = \beta_1^8 \left[\nu_8^1 \Sigma_{f8}^1 \psi^1 + \nu_8^2 \Sigma_{f8}^2 \psi^2 \right] - \lambda_1^8 \psi^3 \quad , \tag{2.3.19}$$

$$\frac{\partial \psi^4}{\partial t} = \beta_2^8 \left[\nu_8^1 \Sigma_{f8}^1 \psi^1 + \nu_8^2 \Sigma_{f8}^2 \psi^2 \right] - \lambda_2^8 \psi^4 \quad , \tag{2.3.20}$$

$$\frac{\partial \psi^5}{\partial t} = \beta_1^9 \left[\nu_9^1 \Sigma_{f9}^1 \psi^1 + \nu_9^2 \Sigma_{f9}^2 \psi^2 \right] - \lambda_1^9 \psi^5 \quad , \text{ and} \tag{2.3.21}$$

$$\frac{\partial \psi^6}{\partial t} = \beta_2^9 \left[\nu_9^1 \Sigma_{f9}^1 \psi^1 + \nu_9^2 \Sigma_{f9}^2 \psi^2 \right] - \lambda_2^9 \psi^6 \quad , \tag{2.3.22}$$

where

$$\psi^1 = \frac{\partial \phi^1}{\partial \alpha_i} \quad ,$$

$$\psi^2 = \frac{\partial \phi^2}{\partial \alpha_i} \quad ,$$

$$\psi^3 = \frac{\partial C_1^8}{\partial \alpha_i} \quad ,$$

$$\psi^4 = \frac{\partial C_2^8}{\partial \alpha_i} \quad ,$$

$$\psi^5 = \frac{\partial C_1^9}{\partial \alpha_i} \quad ,$$

$$\psi^6 = \frac{\partial C_2^9}{\partial \alpha_i} \quad ,$$

$$\theta^{g}_{j,k} = \frac{\partial \chi^{g}_{j,k}}{\partial \alpha_i} = \begin{cases} 1 \text{ if } \chi^{g}_{j,k} = \alpha_i \\ 0 \text{ otherwise} \end{cases}, \quad (j = 1, 2;\ k = 8,9;\ g = 1,2), \text{ and}$$

$$C^{g}_{j}(\underline{\alpha}_0) = C^{g}_{j}(r,t;\ \underline{\alpha}_0)$$

= precursor concentrations found by solving equations (2.3.1) to (2.3.6) using the unperturbed parameter vector $\underline{\alpha}_0$.

The Fréchet derivative of the state vector $\underline{X}$, with respect to the parameter α_i, may then be written as

$$\underline{\psi} = \partial \underline{X} / \partial \alpha_i = (\psi^1, \psi^2, \psi^3, \psi^4, \psi^5, \psi^6) \ . \tag{2.3.23}$$

The initial and boundary conditions for equations (2.3.17) to (2.3.22) are given by

$$\left.\frac{\partial \psi^1}{\partial r}\right|_{r=0} = 0 \ ; \ \psi^1(r = R) = 0 \ ; \ \psi^1(t = 0) = \psi^1_0 \ , \tag{2.3.24}$$

$$\left.\frac{\partial \psi^2}{\partial r}\right|_{r=0} = 0 \ ; \ \psi^2(r = R) = 0 \ ; \ \psi^2(t = 0) = \psi^2_0 \ , \tag{2.3.25}$$

$$\psi^3(t = 0) = \frac{\beta^8_1}{\lambda^8_1}\left[\nu^1_8 \Sigma^1_{f8} \psi^1_0 + \nu^2_8 \Sigma^2_{f8} \psi^2_0\right] = \psi^3_0 \ , \tag{2.3.26}$$

$$\psi^4(t = 0) = \frac{\beta^8_2}{\lambda^8_2}\left[\nu^1_8 \Sigma^1_{f8} \psi^1_0 + \nu^2_8 \Sigma^2_{f8} \psi^2_0\right] = \psi^4_0 \ , \tag{2.3.27}$$

$$\psi^5(t = 0) = \frac{\beta^9_1}{\lambda^9_1}\left[\nu^1_9 \Sigma^1_{f9} \psi^1_0 + \nu^2_9 \Sigma^2_{f9} \psi^2_0\right] = \psi^5_0 \ , \text{ and} \tag{2.3.28}$$

$$\psi^6(t = 0) = \frac{\beta_2^9}{\lambda_2^9}\left[\nu_9^1\Sigma_{f9}^1\psi_0^1 + \nu_9^2\Sigma_{f9}^2\psi_0^2\right] = \psi_0^6 \ . \qquad (2.3.29)$$

These were determined by taking the Fréchet derivatives of equations (2.3.10) to (2.3.15) with respect to α_i.

It should be noted that the operators acting on $\underline{X}$ and $\underline{\psi}$ respectively, are identical. This is the case since the original system of equations, (2.3.1) to (2.3.6), is linear. Also, since the Fréchet derivatives, rather than the differentials, of equations (2.3.1) to (2.3.6) were taken, equations (2.3.17) to (2.3.22) do not quite fit the form of equation (2.2.9). Using derivatives, equation (2.2.9) would have the form

$$\underline{\underline{L}}\ \underline{\underline{X}}'_{\underline{\alpha}} = \underline{\underline{S}}, \qquad (2.3.30)$$

where $\underline{\underline{L}}$ and $\underline{\underline{S}}$ have the same definition as in equation (2.2.9), and $\underline{\underline{X}}'_{\underline{\alpha}}$ is a matrix representing the Fréchet derivative of the state vector $\underline{X}$ with respect to the parameter vector $\underline{\alpha}$. Since, in deriving equations (2.3.17) and (2.3.22), differentiation was performed with respect to the i-th component of the parameter vector $\underline{\alpha}$, equation (2.3.30) becomes

$$\underline{\underline{L}}\underline{\psi} = \underline{S}^i \ , \qquad (2.3.31)$$

where

$\underline{\psi} = \partial\underline{X}/\partial\alpha_i$ (the i-th column of $\underline{\underline{X}}'_{\underline{\alpha}}$), and

$\underline{S}^i$ = i-th column of $\underline{\underline{S}}$.

Equations (2.3.17) to (2.3.22) fit the form of equation (2.3.31).

Adjoint System to $\underline{\underline{L}}\,\underline{\psi} = \underline{S}^i$

The solution of the system of equations adjoint to (2.3.31) is required to calculate the variation in the responce as given in equation (2.2.17). Actually, since derivatives were used in the above development instead of differentials, equation (2.2.17) becomes an explicit expression for the sensitivity derivatives. Using equation (2.2.11) and again using Fréchet derivatives rather than differentials, the adjoint operator $\underline{\underline{L}}^*$, adjoint to $\underline{\underline{L}}$, can be defined by

$$\langle \underline{\underline{L}}^* \underline{\Phi}, \underline{\psi} \rangle = \langle \underline{\Phi}, \underline{\underline{L}}\underline{\psi} \rangle + P[\underline{\Phi}, \underline{\psi}] \ , \tag{2.3.32}$$

where $\underline{\Phi}$ is adjoint to $\underline{\psi}$. Following the procedure for finding $\underline{\underline{L}}^*$, described in section 2.2, the equations adjoint to equations (2.3.17) to (2.3.22) are obtained. The adjoints to equations (2.3.17) and (2.3.18) are

$$\begin{aligned}
&D^1 \nabla^2 \Phi^1 - \left[\Sigma_a^1 + \Sigma_p^1 + \Sigma_S^{1/2} + D^1 B_z^2\right] \Phi^1 \\
&+ \chi_p^1 \left[(1 - \beta^8)\nu_8^1 \Sigma_{f8}^1 + (1 - \beta^9)\nu_9^1 \Sigma_{f9}^1 + (\nu\Sigma_f)_1^*\right] \Phi^1 \\
&+ \chi_p^2 \left[(1 - \beta^8)\nu_8^1 \Sigma_{f8}^1 + (1 - \beta^9)\nu_9^1 \Sigma_{f9}^1 + (\nu\Sigma_f)_1^*\right] \Phi^2 \\
&+ \Sigma_S^{1/2} \Phi^2 \\
&+ \beta_1^8 \nu_8^1 \Sigma_{f8}^1 \Phi^3 + \beta_2^8 \nu_8^1 \Sigma_{f8}^1 \Phi^4 + \beta_1^9 \nu_9^1 \Sigma_{f9}^1 \Phi^5 + \beta_2^9 \nu_9^1 \Sigma_{f9}^1 \Phi^6 = f(r,t),
\end{aligned} \tag{2.3.33}$$

and

$$D^2\nabla^2\Phi^2 - \left[\Sigma_a^2 + \Sigma_p^2 + D^2B_z^2\right]\Phi^2$$

$$+ \chi_p^2\left[(1-\beta^8)\nu_8^2\Sigma_{f8}^2 + (1-\beta^9)\nu_9^2\Sigma_{f9}^2 + (\nu\Sigma_f)_2^*\right]\Phi^2$$

$$+ \chi_p^1\left[(1-\beta^8)\nu_8^2\Sigma_{f8}^2 + (1-\beta^9)\nu_9^2\Sigma_{f9}^2 + (\nu\Sigma_f)_2^*\right]\Phi^1$$

$$+ \beta_1^8\nu_8^2\Sigma_{f8}^2\Phi^3 + \beta_2^8\nu_8^2\Sigma_{f8}^2\Phi^4 + \beta_1^9\nu_9^2\Sigma_{f9}^2\Phi^5 + \beta_2^9\nu_9^2\Sigma_{f9}^2\Phi^6 = g(r,t) \quad . \qquad (2.3.34)$$

The adjoints to equations (2.3.19) to (2.3.22) are

$$\frac{\partial\Phi^3}{\partial t} = \lambda_1^8\Phi^3 - \left[\lambda_1^8\chi_{1,8}^1\Phi^1 + \lambda_1^8\chi_{1,8}^2\Phi^2\right], \qquad (2.3.35)$$

$$\frac{\partial\Phi^4}{\partial t} = \lambda_2^8\Phi^4 - \left[\lambda_2^8\chi_{2,8}^1\Phi^1 + \lambda_2^8\chi_{2,8}^2\Phi^2\right], \qquad (2.3.36)$$

$$\frac{\partial\Phi^5}{\partial t} = \lambda_1^9\Phi^5 - \left[\lambda_1^9\chi_{1,9}^1\Phi^1 + \lambda_1^9\chi_{1,9}^2\Phi^2\right], \text{ and} \qquad (2.3.37)$$

$$\frac{\partial\Phi^6}{\partial t} = \lambda_2^9\Phi^6 - \left[\lambda_2^9\chi_{2,9}^1\Phi^1 + \lambda_2^9\chi_{2,9}^2\Phi^2\right] . \qquad (2.3.38)$$

In the process of deriving $\underline{\underline{L}}^*$ (Appendix 2) the following boundary and final conditions are obtained:

$$\underline{\Phi}(r,\ t_f;\ \underline{\alpha}_0) = 0 \ , \qquad (2.3.39)$$

$$\underline{\Phi}(R,\ t;\ \underline{\alpha}_0) = 0 \ , \text{ and} \qquad (2.3.40)$$

$$\left.\frac{\partial\underline{\Phi}}{\partial r}\right|_{r=0} = 0 \ . \qquad (2.3.41)$$

Sensitivity Derivatives

Again, rather than using differentials, as in equation (2.2.17), taking Fréchet derivatives results in equation (2.2.17) taking the form

$$\left.\frac{dR}{d\alpha_i}\right|_{\underline{\alpha}_0} = \left.\frac{\partial R}{\partial \alpha_i}\right|_{\underline{\alpha}_0} + \left.\langle \underline{\Phi}, \underline{S}^i \rangle\right|_{\underline{\alpha}_0} + \left.\hat{P}[\underline{\Phi},\underline{\psi}]_{\underline{\alpha}_0}\right|_{\underline{\alpha}_0} , \tag{2.3.42}$$

where each term is evaluated at $\underline{\alpha} = \underline{\alpha}_0$, all derivatives are with respect to the i-th component of the parameter vector, and $\underline{\Phi}$ is adjoint to $\underline{\psi}$. Further, since the weight functions in equation (2.3.16) are independent of the parameters, the direct effect term, $\partial R/\partial \alpha_i$, is identically zero, so equation (2.3.42) reduces to

$$\left.\frac{dR}{d\alpha_i}\right|_{\underline{\alpha}_0} = \left.\langle \underline{\Phi}, \underline{S}^i \rangle\right|_{\underline{\alpha}_0} + \left.\hat{P}[\underline{\Phi},\underline{\psi}]_{\underline{\alpha}_0}\right|_{\underline{\alpha}_0} . \tag{2.3.43}$$

$\underline{\Phi}(r,t;\ \underline{\alpha}_0)$ is obtained by solving the adjoint system of equations (2.3.33) to (2.3.38) and $\underline{S}^i(r,t;\ \underline{\alpha}_0)$ is obtained by evaluating the right hand sides of equations (2.3.17) and (2.3.18) using the solutions of equations (2.3.1) to (2.3.6). Only the first two components of $\underline{S}^i$ are non-zero. These are tabulated in table 2.3.1. The bilinear concomitant, $\hat{P}[\underline{\Phi},\underline{\psi}]$, arises from the integration of terms containing first derivatives with respect to time. Details of the derivation of the bilinear concomitant are given in Appendix 2. Equation (2.3.43) becomes

$$\left.\frac{dR}{d\alpha_i}\right|_{\alpha_0} = 2\pi H \int_0^{t_f}\int_0^{R} \left[\Phi^1(r,t;\underline{\alpha}_0)S_1^i(r,t;\underline{\alpha}_0) + \Phi^2(r,t;\underline{\alpha}_0)S_2^i(r,t;\underline{\alpha}_0)\right]rdrdt$$

$$- 2\pi H \int_0^{R} \psi^3(r,0;\underline{\alpha}_0)\ \Phi^3(r,0;\underline{\alpha}_0)rdr$$

$$- 2\pi H \int_0^{R} \psi^4(r,0;\underline{\alpha}_0)\ \Phi^4(r,0;\underline{\alpha}_0)rdr$$

$$- 2\pi H \int_0^{R} \psi^5(r,0;\underline{\alpha}_0)\ \Phi^5(r,0;\underline{\alpha}_0)rdr$$

$$- 2\pi H \int_0^{R} \psi^6(r,0;\underline{\alpha}_0)\ \Phi^6(r,0;\underline{\alpha}_0)rdr\ , \qquad (2.3.44)$$

where $\psi^3(r,0;\underline{\alpha}_0)$, .. , $\psi^6(r,0;\underline{\alpha}_0)$ are found by solving the steady-state form of equations (2.3.17) to (2.3.22). Then, for a given variation $\delta\underline{\alpha}$, the variation in the responce can be found by the inner product

$$\delta R = \frac{dR}{d\underline{\alpha}} \cdot \delta\underline{\alpha}\ . \qquad (2.3.45)$$

Table 2.3.1

Explicit Forms of the First Two Components

of $\underline{S}^{i}(r,t;\underline{\alpha}_0)$ in Equation (2.3.31)

i	α_i	$S_1^i(r,t;\underline{\alpha}_0)$	$S_2^i(r,t;\underline{\alpha}_0)$
1	$\chi^1_{1,8}$	$-\lambda_1^8 c_1^8(r,t;\underline{\alpha}_0)$	0
2	$\chi^2_{1,8}$	0	$-\lambda_1^8 c_1^8(r,t;\underline{\alpha}_0)$
3	$\chi^1_{1,9}$	$-\lambda_1^9 c_1^9(r,t;\underline{\alpha}_0)$	0
4	$\chi^2_{1,9}$	0	$-\lambda_1^9 c_1^9(r,t;\underline{\alpha}_0)$
5	$\chi^1_{2,8}$	$-\lambda_2^8 c_2^8(r,t;\underline{\alpha}_0)$	0
6	$\chi^2_{2,8}$	0	$-\lambda_2^8 c_2^8(r,t;\underline{\alpha}_0)$
7	$\chi^1_{2,9}$	$-\lambda_2^9 c_2^9(r,t;\underline{\alpha}_0)$	0
8	$\chi^2_{2,9}$	0	$-\lambda_2^9 c_2^9(r,t;\underline{\alpha}_0)$

Chapter 3

FORWARD PROBLEM

3.1 Model

3.1.1 Introduction

In this study, the transient behaviour of an LMFBR is to be modelled. The transients will be induced by time-varying reactivity insertions. This will be done by including user-defined subroutines in the computer program for solving the forward problem (reactor kinetics equations). Programmed into the subroutines will be time-varying poison cross sections for the region(s) of the core containing control rods. Reducing the poison cross sections in these regions will simulate ejection or withdrawal of the control rods, while increasing the cross sections will simulate insertion of the rods.

Specific transients will be discussed later when discussing the specifics of the sensitivity analysis.

3.1.2 Type of Reactor Being Modelled

The reference design MOX-fuelled LMFBR used in the INFCE study is used as the basis for this study. The reference design characteristics for the reactor are summarised in table 3.1.1. The core and radial blanket layout is shown in figure 3.1.1. The MOX core composition is taken to be the initial loading composition for a new core [12], and similarly for the blanket. The core and blanket compositions are

summarised in table 3.1.2.

3.1.3 Data Preparation

(a) Geometrical Data

The geometry of the MOX fuel assemblies, blanket assemblies and control rod assemblies is given in table 3.1.1. Since the diameter of the reactor is large compared to that of an individual assembly (≃ 12 to 1), the reactor may be modelled as a cylinder. The control assembly in the centre of the core was also modelled as a cylinder of diameter equivalent to the assembly pitch. The relationship between the actual core geometry and that used in the model is shown in figure 3.1.2.

(b) Reactor Materials

The MOX fuel, depleted uranium blanket and B_4C control material are clad in type 306 stainless steel (SS-306). The MOX fuel is made from recycled plutonium and the blanket fuel is made entirely from depleted uranium. The coolant material is pure (liquid) sodium (Na-23) and the control material is B_4C. Details of the fuel composition are given in table 3.1.2.

(c) Cross Section Generation

Most of the cross section data required were generated using the Monte Carlo code VIM [15]. The VIM code was specifically designed for

Table 3.1.1

Some Characteristics of the INFCE Reference Design MOX-Fuelled LMFBR

(From reference 12)

General Reactor Data	
Electrical Output, MWe	1000
Thermal Output, MWt	2740
Core Height, cm	101.6
No. of Assemblies	
Inner Core	180
Outer Core	138
Control	19
Radial Blanket	234
Fuel Design Data	
Fuel Material	$Pu\text{-}UO_2$
Pin O.D., cm	0.7366
Clad Thickness, cm	0.0356
Pitch/Diameter Ratio	1.186
Assembly Design	
No. of Pins	271
Assembly Pitch, cm	16.0274

Table 3.1.1
(continued)

Radial Blanket Assembly

Fuel Material	UO_2
Duct Outside Flat-to-Flat, cm	46.025
No. of Pins	127
Pin O.D., cm	1.1938
Clad Thickness, cm	0.0381
Pitch/Diameter Ratio	1.070

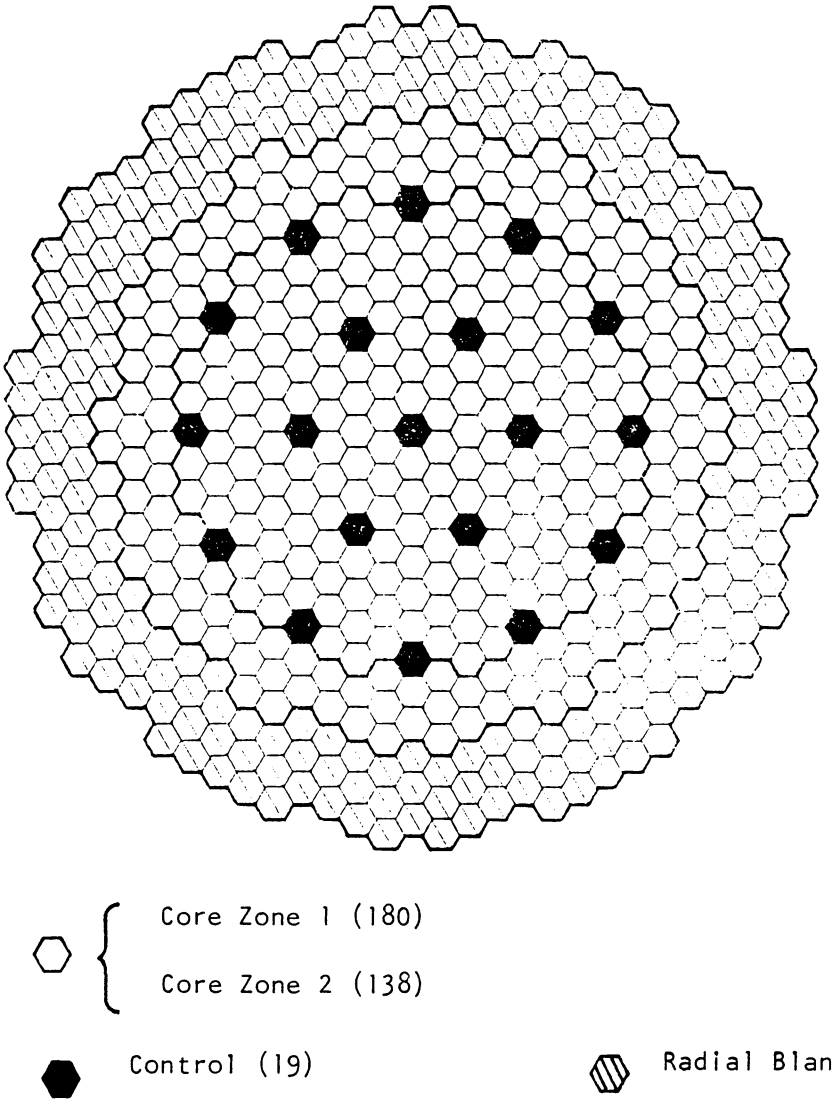

Fig. 3.1.1 Core Layout for INFCE Reference Design MOX-Fuelled LMFBR. (From reference 12)

Table 3.1.2

Initial Fuel Loading of the INFCE Reference Design MOX-Fuelled LMFBR

(From reference 12)

Core	
U-235	44.6 kg
U-238	22544.0
Pu-238	40.4
Pu-239	2728.9
Pu-240	781.8
Pu-241	413.0
Pu-242	98.5
Radial Blanket	
U-235	90.0 kg
U-238	44890.0

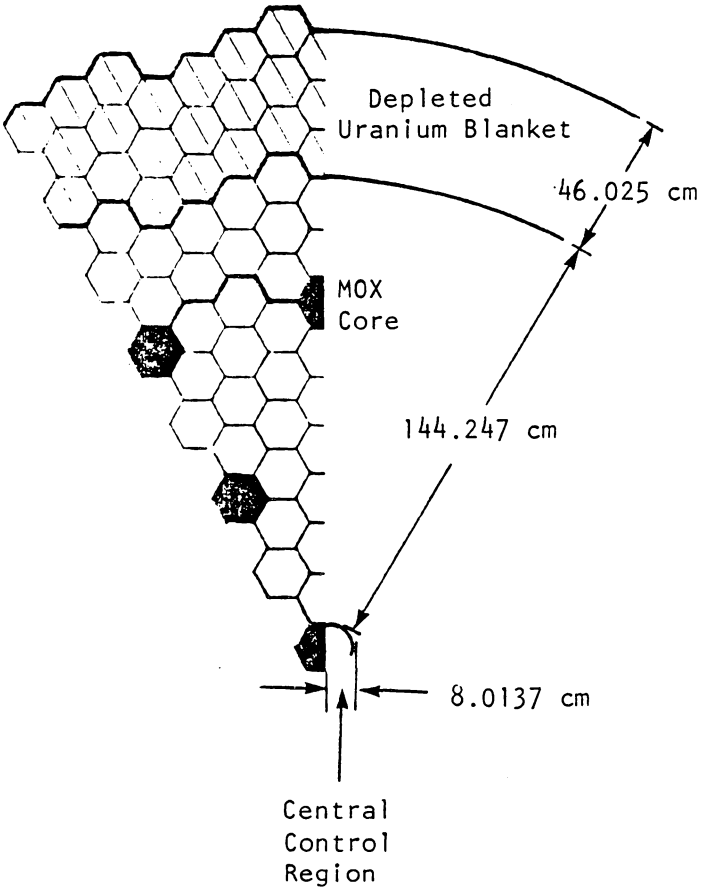

Fig. 3.1.2 Conversion of Core Geometry to an Equivalent Cylindrical Geometry.

fast reactor criticality studies. It has a neutron physics data base derived from ENDF-B/IV [16]. The VIM data base contains pointwise cross section data with linear interpolation for resonance and smooth cross sections. This provides a continuous energy cross section description. A probability table method [15] is used to describe the unresolved resonances. The VIM code also has a wide range of geometrical capabilities.

The VIM code calculates the multiplication factor, reaction rates, and multigroup cross sections for each isotope and geometric region in the problem. Any multigroup structure may be chosen in the energy range from 20 MeV to 10^{-5} eV. The VIM output may then be retallied by collapsing groups and regions into whatever form the user desires.

Two separate VIM calculations were made. The first was to generate cross sections for the MOX core. The core was simulated by an infinite array of unit cells with a zero-current boundary condition on all boundaries. Similarly, an infinite-lattice unit-cell calculation was performed for the blanket. No poison material was included in the calculation for the MOX core.

A 55-group energy scheme was used. Allowing the Monte Carlo calculation run until about 600,000 collisions were recorded produced microscopic cross sections with two standard deviation uncertainties of about 1%. The multigroup data were collapsed to two-group data with the group boundary being 0.11 MeV. The reason for such a choice was that about 50% of all neutron interactions occur in each of the two groups. The fuel, clad, and coolant regions were homogenised into a single

region.

The VIM cross section library contains cross section data for the fuel isotopes at 300 and 1000°K respectively. All other data are at 300°K. The VIM calculations were performed using both sets of cross sections. It was found that there is no significant difference between the two resulting sets of two-group data, so the 300°K data were used exclusively.

Absorption, fission, production, scattering and total cross sections are given directly by VIM. Diffusion coefficients were calculated using the scattering and total cross sections as follows:

$$D_g = \frac{1}{3\Sigma^g_{tr}}, \tag{3.1.1}$$

where

$$\Sigma^g_{tr} = \sum_i (\Sigma^g_t - \bar{\mu}_o \Sigma^g_S)_i$$

$= $ transport cross section in group g,

Σ^g_t = total cross section in group g,

Σ^g_S = elastic scattering cross section in group g,

$\bar{\mu}_o$ = mean cosine of the scattering angle, and

$\sum_i$ = summation over all isotopes.

The transfer cross section from group 1 to group 2 is given by

$$\Sigma^{1/2}_S = \frac{\chi^1_p \text{ (total production rate)} - \text{(absorption rate in group 1)}}{\text{group 1 flux}}. \tag{3.1.2}$$

In the central region of the core, pure sodium is present when the control assembly is fully ejected. The transport and group transfer data for sodium were obtained by collapsing the 16-group cross sections from ANL-5800 [17] using the group fluxes from the VIM calculation for the MOX core.

The number densities of all materials used in the VIM calculations are summarised in Appendix 3. The derived diffusion data for each region of the reactor are summarised in Appendix 4.

(d) Delayed Neutron Data

Delayed neutron yields, spectra, and precursor decay constants are required for performing the transient analysis. The delayed neutrons are classically grouped into six groups. However, to simplify the analysis, the six groups were collapsed into two groups, viz, groups one, two, and three were lumped into one group, and groups four, five, and six were lumped into one group also. The new groups shall be referred to as groups one and two.

The delayed neutron yields were obtained from compilations of data made by Keepin [18] for fast fission. Yields for the two delayed neutron groups of U-238 and Pu-239 were found. To check these data, the effective delayed neutron fraction for the reactor was calculated. A value of 0.00326 was obtained which compares favourably with the value of 0.00365 used in the CRBR PSAR [19].

The decay constants and half-lives of the two delayed neutron precursor groups were found by yield weighting the inverse decay

constants of the individual components of the groups. The half-lives of delayed neutron precursor groups one and two are 14 and 1.3 seconds respectively for U-238 and 17 and 1.5 seconds respectively for Pu-239.

The delayed neutron spectra were also obtained from Keepin. Values of 0.83 and 0.17 respectively were selected for energy groups one and two without regard for the fissioning isotope from which the neutrons originated. The accuracy of the choice of spectra is not of prime importance since the purpose of this entire study is to determine the sensitivity of transient calculations to variations in the spectra.

A summary of all the delayed neutron data is given in Appendix 5.

3.2 Numerics

3.2.1 Model of Reactor

The reactor was modelled by three homogeneous regions:

(1) a central control region (CCR) containing the central control rod assembly,

(2) the MOX region containing the MOX fuel and other control assemblies, and

(3) the depleted uranium radial blanket.

A schematic of the core model is shown in figure 3.2.1.

3.2.2 Determination of Initial Conditions

(a) Governing Equations

The initial conditions are determined by solving the steady-state

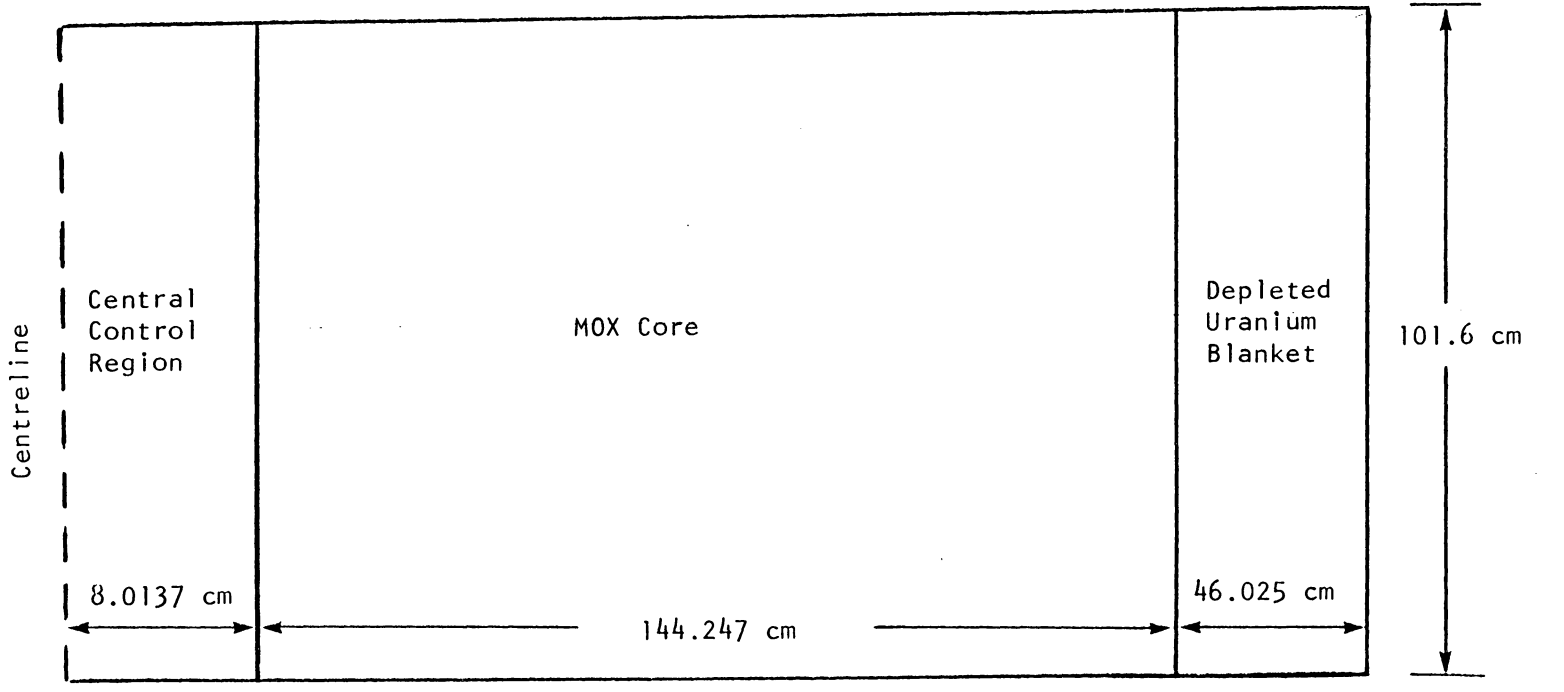

Fig. 3.2.1 Three-Region Model of Core. (Not to Scale)

form of equations (2.3.1) to (2.3.6). If the steady-state form of equations (2.3.3) to (2.3.6) are substituted into equations (2.3.1) and (2.3.2), the steady-state problem reduces to the two-group diffusion equations for $\phi^1(r,0;\underline{\alpha}_o)$ and $\phi^2(r,0;\underline{\alpha}_o)$, respectively. Note that these two-group fluxes are evaluated using the unperturbed parameter vector $\underline{\alpha}_o$.

(b) Differencing Scheme

The two-group diffusion equations were finite differenced using a central difference scheme for the radial component of the Laplacian. The details of the finite-differnce approximation of the Laplacian are given in Appendix 6.

Each of the three regions of the reactor was divided into ten intervals giving a total of 31 spatial mesh points. The mesh points within any one of the regions are equally spaced.

(c) Matrix Form of Equations

The steady-state two-group diffusion equations may be written, using matrix notation, in the following form:

$$\underline{\underline{M}}\ \underline{\phi} = \frac{1}{K}\ \underline{\underline{F}}\ \underline{\phi}\ , \qquad (3.2.1)$$

where

K = the eigenvalue equivalent to the effective multiplication factor,

$\underline{\phi}$ = the eigenvector whose components are $\phi^1(r,0;\underline{\alpha}_o)$ and $\phi^2(r,0;\underline{\alpha}_o)$,

$\underline{\underline{F}}$ = a (2n x 2n) matrix containing only fission source terms,

$\underline{\underline{M}}$ = a (2n x 2n) matrix containing all other terms in the steady-state two-group equations,

and

n = the number of spatial mesh points.

The symmetry condition at the centre of the reactor and the zero-flux boundary condition at the edge of the reactor are included in the difference equations. Details of how the Laplacian was differenced at the centre of the reactor are given in Appendix 6.

Equation (3.2.1) maybe written as

$$\underline{\underline{A}}\ \underline{\phi} = K\ \underline{\phi}\ , \tag{3.2.2}$$

where

$$\underline{\underline{A}} = \underline{\underline{M}}^{-1}\ \underline{\underline{F}}\ . \tag{3.2.3}$$

The eigenvalue equation (3.2.2) was solved using the International Mathematical and Statistical Library (IMSL) subroutine EIGRF [20]. The eigenvalue of largest magnitude and the corresponding eigenvector are the desired solutions.

(d) Criticality Search

Since the reactor will be critical just prior to the transient, the largest eigenvalue of equation (3.2.2) must be unity. A poison is

uniformly distributed throughout the central control region and the MOX region. While the poison is uniformly distributed within each region, its concentration may vary from one region to the other. The poison is represented by specifying a macroscopic poison cross section for each region. By adjusting the poison cross section, the desired critical condition can be achieved. A computer code, FORSTAT, (FORward STATic) was written to perform this calculation.

(e) Testing of FORSTAT

Two eigenvalue calculations were performed to test the eigenvalue calculation in FORSTAT against two standards. The standards were the two-group equation for the eigenvalue [21] and the reactor statics code ODMUG [22].

The first test case was a two-group eigenvalue calculation using diffusion data for a typical PWR [21] without control poison. The results are:

K(two-group eqn.) = 1.1332,

K(ODMUG) = 1.1334, and

K(FORSTAT) = 1.1330.

The second test case was an eigenvalue calculation for the MOX core and radial blanket. No control poison was used. The results are:

K(ODMUG) = 1.118 , and

K(FORSTAT) = 1.117 .

In both cases, agreement to four significant digits is excellent.

3.2.3 Solution of Dynamic Forward Equations

(a) Governing Equations

The governing equations are the reactor kinetics equations (2.3.1) to (2.3.6). In this section the numerical methodology and programming logic used to solve these equations will be discussed.

(b) Differencing Scheme

The same differencing scheme was used, as for the steady-state equations, for approximating the Laplacian. A forward differnce approximation was used for the time derivatives. Details of the differencing schemes are given in Appendix 6.

(c) Estimation of Computer Time

To solve the kinetics equations, it is necessary to invert a (2 m x 2 m) matrix at each time step. (2m because of 2 groups and m mesh points). Using 31 mesh points, this means inverting a (62 x 62) matrix. The choice of time step size should be on the order of the prompt neutron lifetime. For a LMFBR, this is about 10^{-7} second. To simulate a transient for 100 seconds say, 10^{9} inversions are required. It takes 0.25 second to invert a (62 x 62) matrix using the International Mathematics and Statistics Library (IMSL) subroutine LINV1F [23] on the IBM-3032 processor. Hence, to simulate a 100-second transient, about 8 years of processing time would be required!

To overcome this problem, the prompt jump approximation [13] is used so that time steps of the order of one second may be used.

(d) Solution Using the Prompt-Jump Approximation

The prompt-jump approximation (PJA) is effected by setting the derivatives $\partial\phi^1/\partial t$ and $\partial\phi^2/\partial t$ to zero in equations (2.3.1) and (2.3.2). This does not have a significant effect on the accuracy of the results provided the size of the time-steps chosen is much larger than the prompt neutron lifetime. The time derivatives in the precursor equations are preserved.

The initial conditions for the solution of the forward equations are obtained from FORSTAT. The solving of the forward equations is performed in two steps:

(1) using the solutions from the n-th time step the solutions of the precursor equations (2.3.3) to (2.3.6) at the (n+1)-st time step are found; then,

(2) upon substituting these solutions into the diffusion equations (2.3.1) and (2.3.2), with the time derivatives set to zero, these equations are solved for the two-group fluxes at the (n+1)-st time step.

During the duration of the transient, the particular form of the solution is determined by the time-dependent reactivity insertion. This is effected by the use of a time-dependent macroscopic poison cross section in the central control region to simulate motion of the central control rod assembly.

(e) Matrix Form of Equations

The precursor equations need not be put into matrix form since they may be solved independently of each other, i.e., they do not require simultaneous solution. However, the diffusion equations must be solved simultaneously for the two-group fluxes at each mesh point, hence a matrix formulation is appropriate.

Let $\underline{\phi}^{(n)}(r, t_n; \underline{\alpha})$, or simply $\underline{\phi}^{(n)}$, be the solution vector containing the two-group fluxes at the n-th time step, viz,

$$\underline{\phi}^{(n)} = \begin{bmatrix} \underline{\phi}^{1(n)} \\ \\ \underline{\phi}^{2(n)} \end{bmatrix} , \tag{3.2.4}$$

where

$\underline{\phi}^{1(n)}$ $\equiv$ the first-group flux vector, and

$\underline{\phi}^{2(n)}$ $\equiv$ the second-group flux vector.

The two vectors are each of dimension (m x 1), where m is the number of spatial mesh points.

Let $\underline{R}^{(n)}$ be a (2m x 1) vector containing all the precursor terms in equations (2.3.1) and (2.3.2), viz,

$$\underline{R}^{(n)} = \begin{bmatrix} \lambda_1^{8}\chi_{1,8}^{1}\underline{c}_1^{8(n)} + \lambda_2^{8}\chi_{2,8}^{1}\underline{c}_2^{8(n)} + \lambda_1^{9}\chi_{1,9}^{1}\underline{c}_1^{9(n)} + \lambda_2^{9}\chi_{2,9}^{1}\underline{c}_2^{9(n)} \\ \\ \lambda_1^{8}\chi_{1,8}^{2}\underline{c}_1^{8(n)} + \lambda_2^{8}\chi_{2,8}^{2}\underline{c}_2^{8(n)} + \lambda_1^{9}\chi_{1,9}^{2}\underline{c}_1^{9(n)} + \lambda_2^{9}\chi_{2,9}^{2}\underline{c}_2^{9(n)} \end{bmatrix} , \tag{3.2.5}$$

where

$\underline{C}_1^{8(n)}$, $\underline{C}_1^{9(n)}$, $\underline{C}_2^{8(n)}$, and $\underline{C}_2^{9(n)}$ are vectors containing the solutions of equations (2.3.3), (2.3.4), (2.3.5), and (2.3.6) respectively at each mesh point at the n-th time step.

Let $\underline{\underline{B}}$ be a (2m x 2m) coefficient matrix whose elements are the coefficients of all the terms, in equations (2.3.1) and (2.3.2), involving the two-group fluxes excluding, of course, the time derivatives because the PJA is being used.

The two-group diffusion equations can then be written as

$$\underline{\underline{B}}^{(n+1)} \; \underline{\phi}^{(n+1)} = \underline{R}^{(n+1)} \; . \tag{3.2.6}$$

The solution of this equation is given by

$$\underline{\phi}^{(n+1)} = \left[\underline{\underline{B}}^{(n+1)}\right]^{-1} \underline{R}^{(n+1)} \; . \tag{3.2.7}$$

A computer code, DYNFOR (DYNamic FORward), was written to solve the precursor and diffusion equations. The IMSL subroutine LINV1F [23] was used to invert the coefficient matrix.

Once a solution has been found for equations (2.3.1) to (2.3.6), the state vector $\underline{X}^{(n)}$ may be constructed.

The algorithm for solving the forward equations is shown in the flowchart in figure 3.2.2.

3.3 Code Verification

Four tests were performed to verify DYNFOR.

3.3.1 Rod Ejection - Step Insertion of Positive Reactivity

An instantaneous rod ejection was simulated at time t = 0 by setting the poison cross section in the central control region to zero. This results in a \$0.49 step insertion of positive reactivity. The behaviour of the resultant power trace was as expected. After the initial rapid jump in power level, the power rose with an asymptotic period of 6.43 seconds.

3.3.2 Sinusoidally Time-Varying Reactivity

A sinusoidally time-varying reactivity, about zero reactivity, was simulated by programming into DYNFOR a sinusoidally time-varying poison cross section, about the critical value, in the central control region. A 5-second period of oscillation was used. As expected, this resulted in a diverging power oscillation [4].

3.3.3 Change in Steady-State Power Level

The initially critical reactor was put on a positive period by reducing the poison cross section in the central control region. The power was allowed to rise for several seconds. The initial critcal value of the poison cross section was restored and the power levelled off at a new steady-state value as expected.

3.3.4 Rod Drop - Step Insertion of Negative Reactivity

A large negative reactivity insertion was simulated by setting the macroscopic poison cross section in the central control region to 10^6. The power dropped off with an observed asymptotic period of -25.6 seconds. The longest lived precursor has a half-life of 17.4 seconds which results in a predicted asymptotic period of -25.1 seconds. There is only a 2% discrepancy in the observed and predicted periods.

Based on the test results, it was concluded that the code DYNFOR is working correctly.

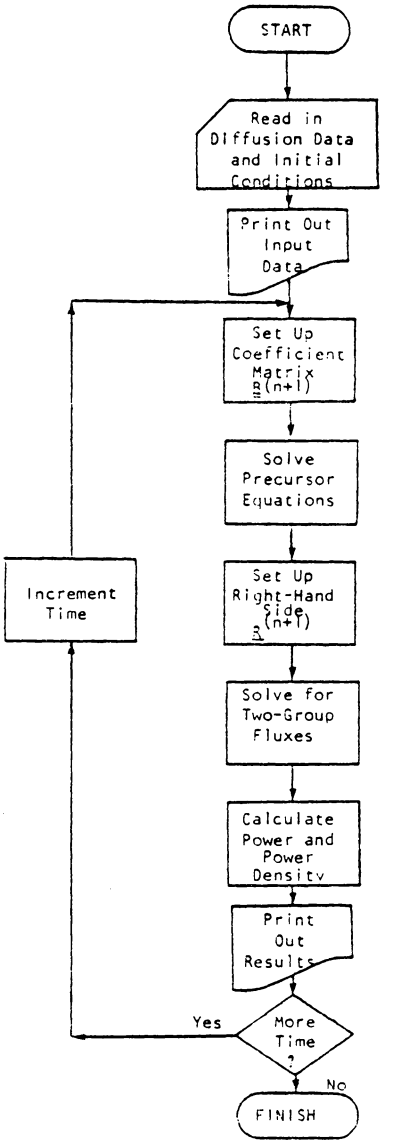

Fig. 3.2.2 Flowchart of the Algorithm Used in the Programme DYNFOR for Solving the Forward Equations.

Chapter 4

ADJOINT PROBLEM

4.1 Introduction

Recall that in order to find the sensitivity derivatives, it is necessary to find the solution to the system of equations that is adjoint to the system (2.3.31). Also recall that equations (2.3.31) arose by taking the Fréchet derivative, with respect to α_i, of the kinetics equations (2.3.1) to (2.3.6). The adjoint equations (2.3.33) to (2.3.38) were derived earlier. The sensitivity derivatives are then evaluated using equations (2.3.44).

Note that all the information in Section 3.1 concerning the modelling of the reactor (i.e., reactor type, geometry, reactor materials, cross sections, and delayed neutron data) holds for the adjoint problem.

4.2 Numerics

4.2.1 Governing Equations

The governing equations for the adjoint problem are given by equations (2.3.33) to (2.3.38) along with the final and boundary conditions given by equations (2.3.39) to (3.2.41). Note that the adjoint system is inhomogeneous whereas the forward equations are homogeneous. Except for the inhomogeneous terms, the general form of the adjoint equations is identical to that of the forward equations. This means that the adjoint equations lend themselves to an identical solution algorithm to that of the forward equations. The major difference in the formulation

of the adjoint problem, as compared to the forward problem, is that the adjoint problem is a final-value problem whereas the forward problem is an initial-value problem.

The adjoint problem can be made into an initial-value problem by redefining the time variable "t" as

$$\tau = t_f - t \ , \tag{4.2.1}$$

where

τ = redefined time variable, and

t_f = final time (i.e., the length of time for which the transient is to be simulated).

The dependent variable, $\underline{\Phi}(r, t; \underline{\alpha}_o)$, of the adjoint equations is redefined by

$$\underline{Z}(r, \tau; \underline{\alpha}_o) = \underline{\Phi}(r, t_f - \tau; \underline{\alpha}_o) = \underline{\Phi}(r, t; \underline{\alpha}_o) \ . \tag{4.2.2}$$

The time derivative is redefined by

$$\frac{\partial \underline{\Phi}}{\partial t} = \frac{\partial \underline{Z}}{\partial \tau} \frac{d\tau}{dt} = - \frac{\partial \underline{Z}}{\partial \tau} \ . \tag{4.2.3}$$

The final condition, $\underline{\Phi}(r, t_f; \underline{\alpha}_o) = 0$, becomes the initial condition $\underline{Z}(r, 0; \underline{\alpha}_o) = 0$. Also, for the same reasons as for the forward problem, the PJA is used to solve the adjoint system.

The above redefinition of variables results in the adjoint equations (2.3.33) to (2.3.38) being transformed into a new system of adjoint equations:

$$D^1\nabla^2 Z^1 - \left[\Sigma_a^1 + \Sigma_p^1 + \Sigma_S^{1/2} + D^1 B_z^2\right] Z^1 + \chi_p^1 \left[(1 - \beta^8)\nu_8^1\Sigma_{f8}^1 + (1 - \beta^9)\nu_9^1\Sigma_{f9}^1 + (\nu\Sigma_f)_1^*\right] Z^1$$

$$+ \Sigma_S^{1/2} Z^2 + \chi_p^2 \left[(1 - \beta^8)\nu_8^1\Sigma_{f8}^1 + (1 - \beta^9)\nu_9^1\Sigma_{f9}^1 + (\nu\Sigma_f)_1^*\right] Z^2$$

$$+ \beta_1^8\nu_8^1\Sigma_{f8}^1 Z^3 + \beta_2^8\nu_8^1\Sigma_{f8}^1 Z^4 + \beta_1^9\nu_9^1\Sigma_{f9}^1 Z^5 + \beta_2^9\nu_9^1\Sigma_{f9}^1 Z^6 = F(r,\tau) \tag{4.2.4}$$

for the faster energy group,

$$D^2\nabla^2 Z^2 - \left[\Sigma_a^2 + \Sigma_p^2 + D^2 B_z^2\right] Z^2 + \chi_p^2 \left[(1 - \beta^8)\nu_8^2\Sigma_{f8}^2 + (1 - \beta^9)\nu_9^2\Sigma_{f9}^2 + (\nu\Sigma_f)_2^*\right] Z^2 + \chi_p^1 \left[(1 - \beta^8)\nu_8^2\Sigma_{f8}^2 + (1 - \beta^9)\nu_9^2\Sigma_{f9}^2 + (\nu\Sigma_f)_2^*\right] Z^1$$

$$+ \beta_1^8\nu_8^2\Sigma_{f8}^2 Z^3 + \beta_2^8\nu_8^2\Sigma_{f8}^2 Z^4 + \beta_1^9\nu_9^2\Sigma_{f9}^2 Z^5 + \beta_2^9\nu_9^2\Sigma_{f9}^2 Z^6 = G(r,\tau) \tag{4.2.5}$$

for the slower energy group,

$$\frac{\partial Z^3}{\partial\tau} = \left[\lambda_1^8\chi_{1,8}^1 Z^1 + \lambda_1^8\chi_{1,8}^2 Z^2\right] - \lambda_1^8 Z^3 \quad , \tag{4.2.6}$$

$$\frac{\partial Z^4}{\partial\tau} = \left[\lambda_2^8\chi_{2,8}^1 Z^1 + \lambda_2^8\chi_{2,8}^2 Z^2\right] - \lambda_2^8 Z^4 \quad , \tag{4.2.7}$$

$$\frac{\partial Z^5}{\partial\tau} = \left[\lambda_1^9\chi_{1,9}^1 Z^1 + \lambda_1^9\chi_{1,9}^2 Z^2\right] - \lambda_1^9 Z^5 \quad , \text{ and} \tag{4.2.8}$$

$$\frac{\partial Z^6}{\partial \tau} = \lambda_2^9 \chi_{2,9}^1 Z^1 + \lambda_2^9 \chi_{2,9}^2 Z^2 - \lambda_2^9 Z^6 \qquad (4.2.9)$$

for the precursors,

where

$$F(r,\tau) = f(r,t_f-\tau) = f(r,t), \text{ and}$$

$$G(r,\tau) = g(r,t_f-\tau) = g(r,t) .$$

The initial and boundary conditions are

$$\underline{Z}(r,0;\underline{\alpha}_o) = 0 ,$$

$$\underline{Z}(R, 0; \underline{\alpha}_o) = 0 , \text{ and}$$

$$\frac{\partial \underline{Z}}{\partial r}\Big|_{r = 0} = 0 .$$

4.2.2 Differencing Scheme

The finite differencing scheme used in solving the adjoint system is identical to that used to solve the forward equations. The differencing scheme is discussed in Appendix 6.

4.2.3 Solution of Equations

The algorithm for solving the adjoint equations is the same as that for the forward problem. Because the PJA is used, the equations have to be solved in two steps:

(1) using the solutions from the n-th time step, the solutions Z^3, Z^4, Z^5 and Z^6 of the adjoint equations (4.2.6) to (4.2.9) at

the (n + 1)-st time step are found; then

(2) upon substituting these solutions into the adjoint equations (4.2.4) and (4.2.5), these equations are solved for Z^1 and Z^2 at the (n + 1)-st time step.

4.2.4 Matrix Form of Equations

As for the forward precursor equations, the adjoint precursor equations need not be put into matrix form since they may be solved independently of each other. The matrix formulation of the two-group adjoint equations is the same as for the forward problem.

Let $\underline{Z}^{(n)}(r, \tau_n; \underline{\alpha}_o)$, or simply $\underline{Z}^{(n)}$, be the solution vector containing the solutions of equations (4.2.4) and (4.2.5) respectively, at the n-th time step, viz,

$$\underline{Z}^{(n)} = \begin{bmatrix} Z^{1(n)} \\ \\ Z^{2(n)} \end{bmatrix} . \qquad (4.2.10)$$

Before putting equations (4.2.4) and (4.2.5) into matrix form, the equations are rearranged so that the left hand sides contain only terms involving Z^1 and Z^2. All other terms are placed on the right hand sides. The right hand sides may be represented by the vector

$$\underline{R}^{(n)} = \begin{bmatrix} F^{(n)} - \beta_1^8 \nu_8^1 \Sigma_{f8}^1 Z^{3(n)} - \beta_2^8 \nu_8^1 \Sigma_{f8}^1 Z^{4(n)} - \beta_1^9 \nu_9^1 \Sigma_{f9}^1 Z^{5(n)} - \beta_2^9 \nu_9^1 \Sigma_{f9}^1 Z^{6(n)} \\ G^{(n)} - \beta_1^8 \nu_8^2 \Sigma_{f8}^2 Z^{3(n)} - \beta_2^8 \nu_8^2 \Sigma_{f8}^2 Z^{4(n)} - \beta_1^9 \nu_9^2 \Sigma_{f9}^2 Z^{5(n)} - \beta_2^9 \nu_9^2 \Sigma_{f9}^2 Z^{6(n)} \end{bmatrix}, \tag{4.2.11}$$

where

$Z^{3(n)}$, $Z^{4(n)}$, $Z^{5(n)}$, and $Z^{6(n)}$ are vectors containing the solutions of equations (4.2.6) to (4.2.9) at the n-th time step.

Let $\underline{\underline{B}}$ be a (2m x 2m) coefficient matrix whose elements are the coefficients of all the terms in equations (4.2.4) and (4.2.5) that involve Z^1 and Z^2. Equations (4.2.4) and (4.2.5) may then be written in matrix form as

$$\underline{\underline{B}}^{(n)} \; \underline{Z}^{(n)} = \underline{R}^{(n)} \; . \tag{4.2.12}$$

The solution of this equation is given by

$$\underline{Z}^{(n)} = \left[\underline{\underline{B}}^{(n)} \right]^{-1} \underline{R}^{(n)} \; . \tag{4.2.13}$$

A computer code, DYNADJ (DYNamic ADJoint), was written to solve the adjoint equations (4.2.6) to (4.2.9) and (4.2.12). The IMSL subroutine LINV1F [23] was used to invert the coefficient matrix.

The algorithm for solving the adjoint equations is shown in the flowchart in figure 4.2.1.

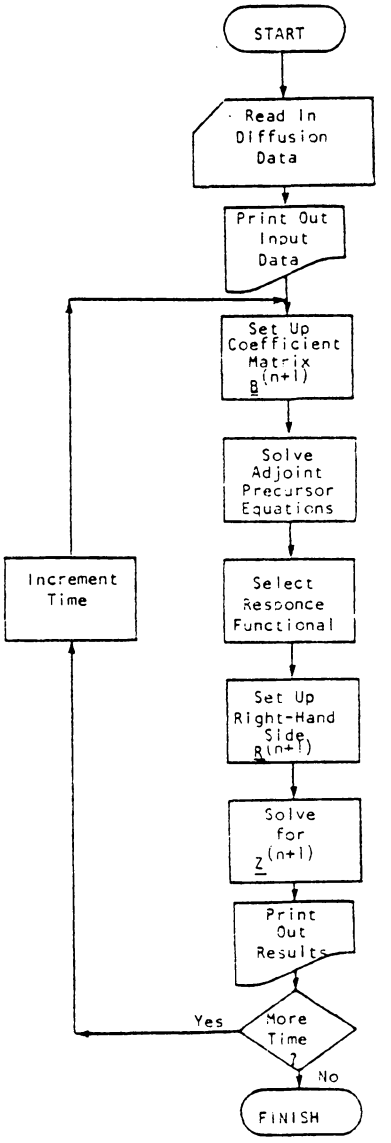

Fig. 4.2.1 Flowchart of the Algorithm Used in the Programme DYNADJ for Solving the Adjoint Equations.

4.3 Code Verification

Verification of DYNADJ is not as easy as for DYNFOR since it is not possible to attach physical meaning to the adjoint solutions. However, the behaviour of the solutions may be predicted using mathematical intuition. Since the system of adjoint equations contains first order time derivatives, and since the system is inhomogeneous, then provided the coefficients (diffusion and delayed neutron parameters) remain unchanged in time, the solutions should behave in a similar fashion to the solution of a first order inhomogeneous differential equation with constant coefficients.

The inhomogeneous terms in the adjoint system contain the weight functions of the responce functional. If these weight functions contain delta functions in time, i.e., $\delta(t - \overline{t})$, then one would expect the solution of the adjoint system to instaneously "jump" to some new value from its initial value and then decay to a new asymptotic value as time approaches infinity.

A delta function was added to the inhomogeneous terms of the equations in DYNADJ and the solutions behaved as anticipated. It was concluded that the code DYNADJ is working correctly.

Chapter 5

Sensitivity Computations

5.1 Model and Problem Statement

The primary, and most difficult task in a sensitivity analysis is to derive a set of sensitivity derivatives. Once these are known, it is a relatively easy task to calculate changes in the system responce for given changes in the parameters. In this study, the system responces are:

(a) the total reactor thermal power at any given instant, $\bar{t}$, during a transient, and

(b) the thermal power density at any instant $\bar{t}$ and radial position $\bar{r}$ in the reactor during a transient. For this study, the radial position of interest is that at which the peak power density occurs.

The responce functional for the power responce is given by

$$P[\bar{t};\ \underline{\alpha}_0] = \int_0^{t_f} \int_0^{R} w_f[\Sigma_f^1\phi^1(r,t;\underline{\alpha}_0) + \Sigma_f^2\phi^2(r,t;\underline{\alpha}_0)]\delta(t-\bar{t})\,2\pi r H dr dt. \tag{5.1.1}$$

The weight functions for the two-group fluxes are

$$f(r,t) = w_f\ \Sigma_f^1\ \delta(t-\bar{t}), \text{ and} \tag{5.1.2}$$

$$g(r,t) = w_f\ \Sigma_f^2\ \delta(t-\bar{t})\ . \tag{5.1.3}$$

The responce functional for the power density responce is given by

$$PD[\bar{r},\bar{t};\underline{\alpha}_0] = \int_0^{t_f} \int_0^{R} w_f[\Sigma_f^1\phi^1(r,t;\underline{\alpha}_0) + \Sigma_f^2\phi^2(r,t;\underline{\alpha}_0)]$$

$$\cdot \frac{\delta(r-\bar{r})\ \delta(t-\bar{t})}{2\pi Hr}\ 2\pi Hr dr dt\ . \qquad (5.1.4)$$

The weight functions for the two-group fluxes are

$$f(r,t) = \frac{w_f\ \Sigma_f^1\ \delta(r-\bar{r})\ \delta(t-\bar{t})}{2\pi Hr}\ , \text{ and} \qquad (5.1.5)$$

$$g(r,t) = \frac{w_f\ \Sigma_f^2\ \delta(r-\bar{r})\ \delta(t-\bar{t})}{2\pi Hr}\ . \qquad (5.1.6)$$

Using these functionals and weights, the sensitivity derivatives $dP/d\alpha_l$ and $dPD/d\alpha_i$ can be calculated. From these, the changes, ΔP and ΔPD, in the power and power density respectively, can be calculated for a given change, $\Delta\underline{\alpha}$, in the parameter vector. Further, knowing the responces $P(\bar{t};\ \underline{\alpha}_0)$ and $PD(\bar{r},\ \bar{t};\ \underline{\alpha}_0)$, evaluated using the unperturbed parameter vector $\underline{\alpha}_0$, and the sensitivity derivatives, the responces $P(\bar{t};\ \underline{\alpha})$ and $PD(\bar{r},\ \bar{t};\ \underline{\alpha})$ can be calculated where $\underline{\alpha} = \underline{\alpha}_0 + \Delta\underline{\alpha}$ is the perturbed parameter vector. The responces are given by

$$P(\bar{t};\ \underline{\alpha}) = P(\bar{t};\ \underline{\alpha}_0) + \Delta P\ , \text{ and}$$

$$PD(\bar{r},\ \bar{t};\ \underline{\alpha}) = PD(\bar{r},\ \bar{t};\ \underline{\alpha}_0) + \Delta PD\ .$$

In this study, the power and power density transients are induced by the ejection of the central control rod assembly. The control rod ejection is simulated by reducing the poison cross section, in the

central control region, from its critical value (i.e., the value of Σ_p required for criticality) to zero. The cross section is reduced linearly in time (ramped). The slope of the ramp is determined by the rod ejection time. Different rod ejection accidents may be studied by varying the rod ejection time. The time dependence of Σ_p is shown in figure 5.1.1.

5.2 Numerics

5.2.1 Analytical Representation of Delta Functions

The weight functions, $f(r,t)$ and $g(r,t)$, described in the previous section contain delta functions. A common representation [24] for the delta function is

$$\delta(z) = \frac{1}{\pi} \lim_{\varepsilon \to 0} \frac{\varepsilon}{z^2 + \varepsilon^2} . \qquad (5.2.1)$$

It should be noted that this representation does possess the following properties of the delta function:

$\delta(z) = 0$ for $z \neq 0$, and

$$\int_{-\infty}^{\infty} \delta(z)\, dz = 1.$$

The above representation was used because it is convenient from a computer programming point of view. The width of the delta function is determined by the choice of the value of ε. The value of ε should be chosen to be much less than the mesh spacing used in the finite differencing scheme. Such a choice of ε ensures that the tails of the

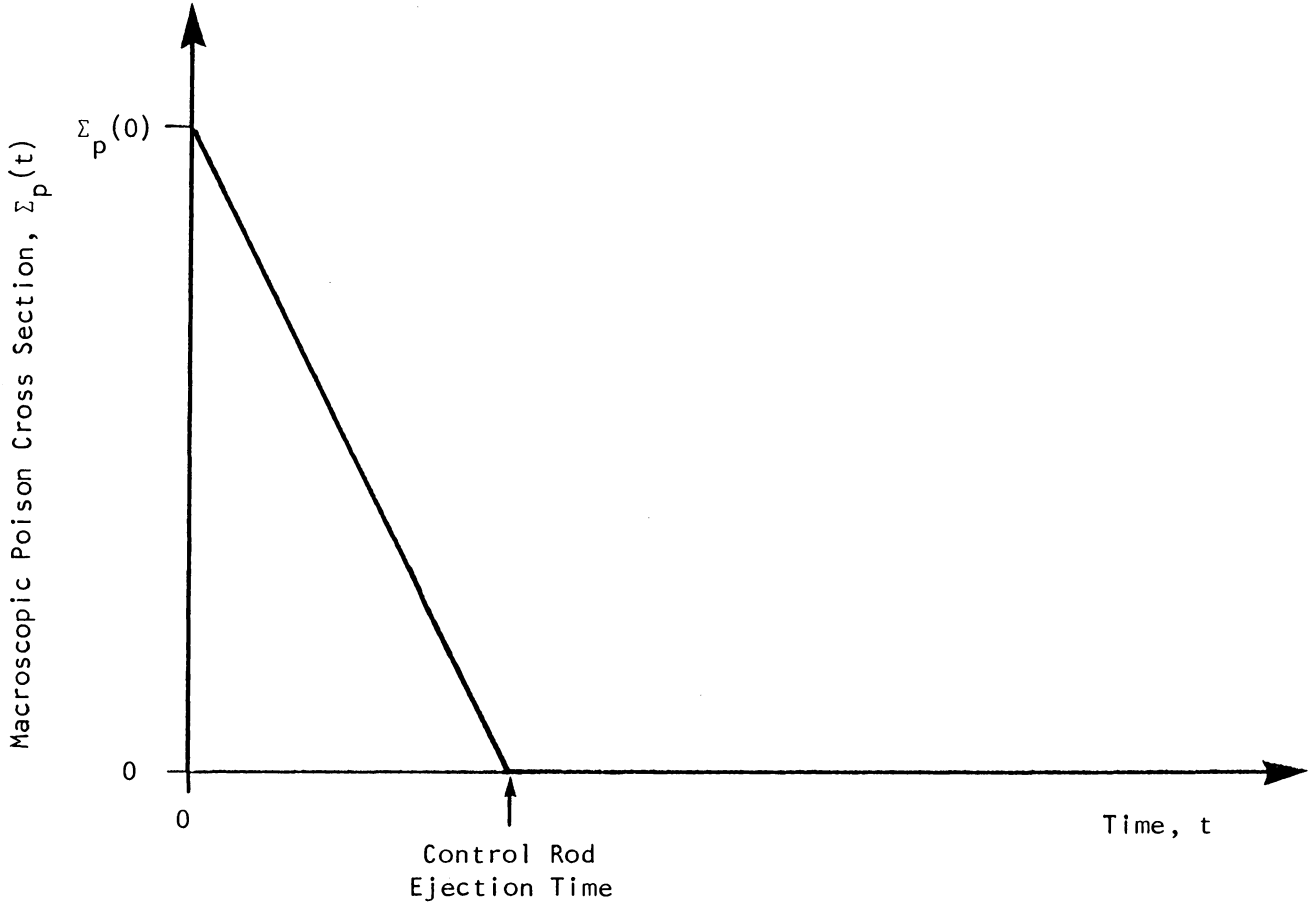

Fig. 5.1.1 Time Dependent Macroscopic Poison Cross Section for Simulating Ejection of Central Control Rod.

analytical representation for the delta function do not spread over adjacent mesh points. This is necessary since the delta function is non-zero only at the mesh point of interest.

5.2.2 Integration Scheme

The calculation of the sensitivity derivatives in equation (2.3.44) involves integrations over space and time. A trapezoidal rule integration scheme was used. Simpson's rule was tried and it was found to have no effect on the results.

5.2.3 Normalisation of Sensitivity Derivatives

The numerical values of the parameters used are given in table 5.2.1. The parameter vector $\underline{\alpha}_0$ is the original unperturbed parameter vector. The changes in $\underline{\alpha}_0$ that were used in this study are:

$$\Delta\underline{\alpha}_2 = - \Delta\underline{\alpha}_1 \ ,$$

$$\Delta\underline{\alpha}_3 = 2\Delta\underline{\alpha}_1 \ ,$$

$$\Delta\underline{\alpha}_4 = 3\Delta\underline{\alpha}_1 \ , \text{ and}$$

$$\Delta\underline{\alpha}_6 = 2\Delta\underline{\alpha}_5 \ .$$

For a given responce, the adjoint equations (2.3.33) to (2.3.38) need to be solved in order to calculate the sensitivity derivatives. The solutions of the adjoint equations are unnormalised, hence the vector of sensitivity derivatives is unnormalised, i.e., the vector

Table 5.2.1 Compilation of Perturbations and Perturbed Parameter Vectors

$\underline{\alpha}$	$\underline{\alpha}_0$	$\Delta\underline{\alpha}_1$	$\underline{\alpha}_1$	$\Delta\underline{\alpha}_2$	$\underline{\alpha}_2$	$\Delta\underline{\alpha}_3$	$\underline{\alpha}_3$	$\Delta\underline{\alpha}_4$	$\underline{\alpha}_4$	$\Delta\underline{\alpha}_5$	$\underline{\alpha}_5$	$\Delta\underline{\alpha}_6$	$\underline{\alpha}_6$
$x^1_{1,8}$	0.83	0.02	0.85	-0.02	0.81	0.04	0.87	0.06	0.89	0.02	0.85	0.04	0.87
$x^2_{1,8}$	0.17	-0.02	0.15	0.02	0.19	-0.04	0.13	-0.06	0.11	-0.02	0.15	-0.04	0.13
$x^1_{1,9}$	0.83	0.02	0.85	-0.02	0.81	0.04	0.87	0.06	0.89	-0.02	0.81	-0.04	0.79
$x^2_{1,9}$	0.17	-0.02	0.15	0.02	0.19	-0.04	0.13	-0.06	0.11	0.02	0.19	0.04	0.21
$x^1_{2,8}$	0.83	0.02	0.85	-0.02	0.81	0.04	0.87	0.06	0.89	0.02	0.85	0.04	0.87
$x^2_{2,8}$	0.17	-0.02	0.15	0.02	0.19	-0.04	0.13	-0.06	0.11	-0.02	0.15	-0.04	0.13
$x^1_{2,9}$	0.83	0.02	0.85	-0.02	0.81	0.04	0.87	0.06	0.89	-0.02	0.81	-0.04	0.79
$x^2_{2,9}$	0.17	-0.02	0.15	0.02	0.19	-0.04	0.13	-0.06	0.11	0.02	0.19	0.04	0.21

contains only the relative values of the sensitivity derivatives. Since the sensitivity derivatives are used to calculate the changes ΔR in the responce R, they must be normalised against a "known" ΔR so as to give the actual, rather than the relative values of the sensitivity derivatives.

In equation (2.3.44), for the sensitivity derivatives, each term contains the adjoint solution. The adjoint solution must be normalised in such a way so as to give the correct values of the sensitivity derivatives. Since the normalisation factor is a common factor in each term in the equation for the sensitivity derivatives, the normalised sensitivity derivatives are obtained by multiplying the unnormalised derivatives by the normalisation factor.

A known ΔR is obtained by calculating the responce $R(\underline{\alpha}_0)$, for the unperturbed parameter vector, and the responce $R(\underline{\alpha})$ for a given perturbed parameter vector. The change in responce is given by $\Delta R = R(\underline{\alpha}) - R(\underline{\alpha}_0)$ for a change in the parameter vector given by $\Delta\underline{\alpha} = \underline{\alpha} - \underline{\alpha}_0$. From a more mathematical standpoint, define the normalisation factor, N, by

$$N = \frac{\Delta R \ (\text{known})}{\Delta R \ (\text{unnormalised})} \ ,$$

where the unnormalised ΔR is calculated using the unnormalised sensitivity derivatives. Then, the normalised sensitivity derivatives are given by

$$\left.\frac{dR}{d\alpha_i}\right|_{\text{normalised}} = \langle N\,\underline{\Phi}, \underline{S}^i\rangle + \hat{P}\,[N\,\underline{\Phi}, \underline{\Psi}]$$

$$= N\langle\underline{\Phi}, \underline{S}^i\rangle + N\,\hat{P}\,[\underline{\Phi}, \underline{\Psi}]$$

$$= N\frac{dR}{d\alpha_i}\Bigg|_{\text{unnormalised}} .$$

It should be noted that it is valid to bring the normalisation factor outside of the bilinear concomitant since the bilinear concomitant is directly proportional to the adjoint $\underline{\Phi}$.

If the responce is changed, then the sensitivity derivatives must be re-normalised to the new responce for the particular transient under consideration. In the case of the power and power density responces $P(\bar{t};\ \underline{\alpha})$ and $PD(\bar{r},\ \bar{t};\ \underline{\alpha})$ respectively, changing $\bar{r}$ and/or $\bar{t}$ constitutes a change in responce.

5.3 Results

5.3.1 Responces Studied

The power and power density responces were discussed in section 5.1. The power responce is evaluated at specified times, $\bar{t}$, after the initiation of the rod ejection transient. The maximum power density responce is evaluated at the same times, $\bar{t}$, as the power responce. In the tables of results that follow, the values of $\bar{t}$ (in seconds) and $\bar{r}$ (in metres), the radial coordinate at which the maximum power density occurs, are specified. Responces were studied for rod ejection accidents with rod ejection times of 2, 10, and 30 seconds.

5.3.2 Sensitivity Derivatives

(a) Power Responce

Recall that the sensitivity derivatives must be normalised against a known change in responce due to a given perturbation, $\Delta\underline{\alpha}$, in the unperturbed parameter vector $\underline{\alpha}_0$. The selection of perturbations for study has been discussed in section 5.2.3 and the values of the perturbed parameters are given in table 5.2.1.

The perturbations $\Delta\underline{\alpha}_2$, $\Delta\underline{\alpha}_3$, and $\Delta\underline{\alpha}_4$ are multiples of the perturbation $\Delta\underline{\alpha}_1$. In order to predict changes in the responce due to $\Delta\underline{\alpha}_2$, $\Delta\underline{\alpha}_3$, and $\Delta\underline{\alpha}_4$, the sensitivity derivatives must be normalised to the change in responce resulting from the perturbation $\Delta\underline{\alpha}_1$. If it is desired to study the change in responce due to a perturbation, $\Delta\underline{\alpha}$, that is not a multiple of $\Delta\underline{\alpha}_1$, the sensitivity derivatives have to be re-normalised. The perturbation $\Delta\underline{\alpha}_6$ is not a multiple of $\Delta\underline{\alpha}_1$. Instead, it is a multiple of $\Delta\underline{\alpha}_5$, hence, to calculate changes in responce due to parameter peiturbations that are multiples of $\Delta\underline{\alpha}_5$, the sensitivity derivatives have to be re-normalised to the change in the responce due to $\Delta\underline{\alpha}_5$.

Notes: (i) The notation $\underline{\alpha}_i$ and α_i will be used. $\underline{\alpha}_i$ represents a particular parameter vector, whereas α_i represents the i-th component of the parameter vector;

(ii) similarly for $\Delta\underline{\alpha}_i$ and $\Delta\alpha_i$.

For simplicity, the notation α_i will be used to represent the components of $\underline{\alpha}$ rather than the notation $\chi^g_{i,j}$ defined in section 2.3.3.

Hence,

$$\underline{\alpha} = (\chi^1_{1,8};\ \chi^2_{1,8};\ \chi^1_{1,9};\ \chi^2_{1,9};\ \chi^1_{2,8};\ \chi^2_{2,8};\ \chi^1_{2,9};\ \chi^2_{2,9})$$

$$= (\alpha_1;\ \alpha_2;\ \alpha_3;\ \alpha_4;\ \alpha_5;\ \alpha_6;\ \alpha_7;\ \alpha_8)\ .$$

The sensitivity derivatives $dP/d\alpha_i$ are presented in tables 5.3.1 to 5.3.6. They have the units of megawatts thermal (MWt). Sensitivity derivatives are tabulated for each rod ejection accident, i.e., for each value of the rod ejection time, and for each normalisation. Recall that the sensitivity derivatives were normalised against known responces due to $\Delta\underline{\alpha}_1$ and $\Delta\underline{\alpha}_5$ respectively.

The first column in the tables contains the components α_i of $\underline{\alpha}$. The remaining four columns contain the corresponding sensitivity derivatives evaluated at the particular times, $\bar{t}$, indicated at the head of each column.

In examining the tables of sensitivity derivatives, the most striking observation is that all the sensitivity derivatives are positive. This is expected since increasing or decreasing α_i would correspondingly increase or decrease the neutron source terms in the diffusion equations resulting in a corresponding increase or decrease in the neutron flux and power. Also, the shorter the rod ejection time, i.e., the more rapid the transient, the larger the sensitivity derivatives as shown in figure 5.3.1. This means that the responce is more sensitive to changes in the parameters during a rapid transient that during a slower transient.

The perturbation, $\Delta\underline{\alpha}$, in the parameter vector is being interpretted

Table 5.3.1 Power Sensitivity Derivatives, $dP/d\alpha_i$, for a Rod Ejection Time of 2 Seconds (Normalised to $\Delta\underline{\alpha}_1$)

α_i	$\bar{t}$ = 10	$\bar{t}$ = 15	$\bar{t}$ = 20	$\bar{t}$ = 25
α_1	225.6	715.6	2034.8	5430.9
α_2	167.5	531.2	1510.4	4031.4
α_3	274.0	891.1	2598.1	7108.8
α_4	203.7	662.4	1931.2	5284.2
α_5	496.8	1572.5	4461.9	11883.7
α_6	368.7	1161.3	3312.0	8821.1
α_7	227.8	726.8	2079.0	5582.5
α_8	169.3	540.2	1545.1	4149.2

Table 5.3.2 Power Sensitivity Derivatives, $dP/d\alpha_i$, for a Rod Ejection Time of 2 Seconds (Normalised to $\Delta\underline{\alpha}_5$)

α_i	$\bar{t}$ = 10	$\bar{t}$ = 15	$\bar{t}$ = 20	$\bar{t}$ = 25
α_1	373.7	1293.2	3931.3	11185.1
α_2	277.4	960.0	2918.2	8302.8
α_3	453.8	1610.4	5019.7	14640.7
α_4	337.3	1197.0	3731.2	10883.0
α_5	822.8	2841.7	8620.6	24474.7
α_6	610.7	2109.4	6398.9	18167.3
α_7	377.2	1313.4	4016.7	11497.3
α_8	280.4	976.1	2985.3	8545.3

Note: $\bar{t}$ has units of seconds.
$dP/d\alpha_i$ has units of MWt.

Table 5.3.3 Power Sensitivity Derivatives, $dP/d\alpha_i$, for a Rod Ejection Time of 10 Seconds (Normalised to $\Delta\underline{\alpha}_1$)

α_i	$\bar{t} = 10$	$\bar{t} = 15$	$\bar{t} = 20$	$\bar{t} = 30$
α_1	68.1	253.0	768.8	5601.1
α_2	50.5	187.8	570.7	4157.6
α_3	83.0	315.5	981.6	7503.5
α_4	61.7	234.5	729.7	5577.5
α_5	149.8	555.8	1685.9	12231.5
α_6	111.2	412.6	1251.4	9078.8
α_7	68.3	255.4	780.7	5756.6
α_8	50.8	189.8	580.3	4278.7

Table 5.3.4 Power Sensitivity Derivatives, $dP/d\alpha_i$, for a Rod Ejection Time of 10 Seconds (Normalised to $\Delta\underline{\alpha}_5$)

α_i	$\bar{t} = 10$	$\bar{t} = 15$	$\bar{t} = 20$	$\bar{t} = 30$
α_1	98.4	408.9	1386.4	11792.7
α_2	73.1	303.5	1029.2	8753.6
α_3	120.0	509.9	1770.2	15798.2
α_4	89.2	379.1	1315.8	11743.0
α_5	216.6	898.4	3040.3	25752.6
α_6	160.8	666.9	2256.7	19114.9
α_7	98.8	412.8	1407.9	12120.2
α_8	73.4	306.8	1046.5	9008.4

Note: $\bar{t}$ has units of seconds.
$dP/d\alpha_i$ has units of MWt.

Table 5.3.5 Power Sensitivity Derivatives, $dP/d\alpha_i$, for a Rod Ejection Time of 30 Seconds (Normalised to $\Delta\underline{\alpha}_1$)

α_i	$\bar{t}$ = 10	$\bar{t}$ = 20	$\bar{t}$ = 30	$\bar{t}$ = 45
α_1	17.9	71.0	446.9	8409.8
α_2	13.3	52.7	331.7	6242.6
α_3	21.9	90.2	592.1	11907.7
α_4	16.3	67.1	440.1	8851.3
α_5	39.4	155.7	976.6	18268.3
α_6	29.3	115.6	724.9	13560.4
α_7	17.9	71.3	452.2	8660.3
α_8	13.3	53.0	336.1	6436.8

Table 5.3.6 Power Sensitivity Derivatives, $dP/d\alpha_i$, for a Rod Ejection Time of 30 Seconds (Normalised to $\Delta\underline{\alpha}_5$)

α_i	$\bar{t}$ = 10	$\bar{t}$ = 20	$\bar{t}$ = 30	$\bar{t}$ = 45
α_1	19.7	104.7	792.0	19321.1
α_2	14.6	77.7	587.9	14342.0
α_3	24.0	133.1	1049.4	27357.3
α_4	17.8	98.9	780.0	20335.5
α_5	43.3	229.7	1730.7	41970.7
α_6	32.1	170.5	1284.7	31154.5
α_7	19.7	105.2	801.4	19896.7
α_8	14.6	78.2	595.6	14788.2

Note: $\bar{t}$ has units of seconds.
$dP/d\alpha_i$ has units of MWt.

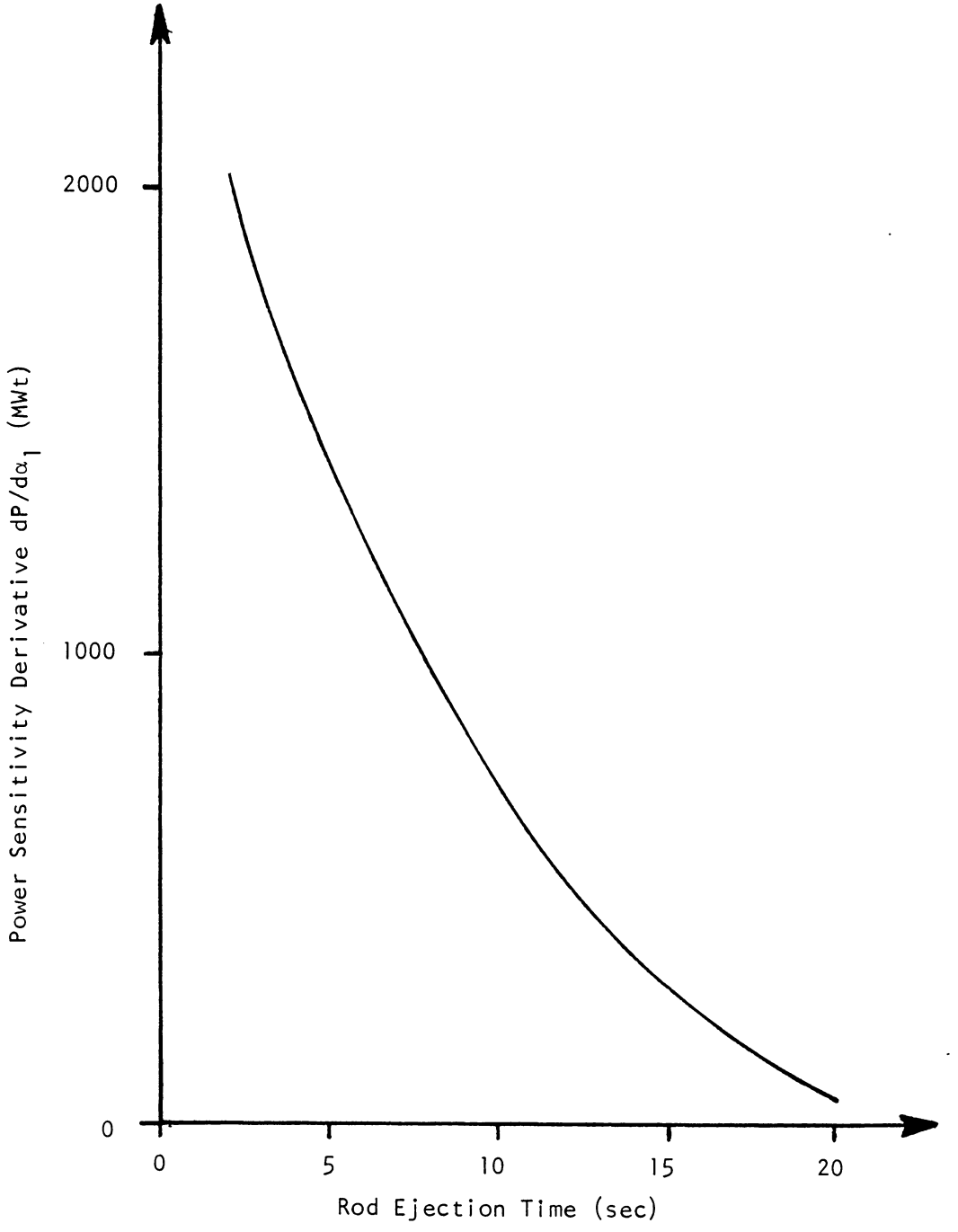

Fig. 5.3.1 Variation of Power Sensitivity Derivative $dP/d\alpha_1$ With Rod Ejection Time 20 Seconds After Initiation of Transient. (Normalised to $\Delta\underline{\alpha}_1$)

as an uncertainty in the parameter vector $\underline{\alpha}_0$, so the change in the power responce, ΔP, is to be interpretted as the uncertainty in the reactor power level. Hence, the more rapid the transient, the larger the uncertainty in power at some time $\bar{t}$ during the transient as compared to the uncertainty at the same time $\bar{t}$ for a more slowly varying transient. Also, during a transient, the uncertainty increases with time.

The sensitivity derivatives may be ranked according to their magnitudes, $dP/d\alpha_5$ is the largest, while $dP/d\alpha_2$ is the smallest. This means that the power responce is most sensitive to changes in $\chi^1_{2,8}$ and least sensitive to changes in $\chi^2_{1,8}$. It should be noted that $dP/d\alpha_1$ and $dP/d\alpha_2$ are essentially the same as $dP/d\alpha_7$ and $dP/d\alpha_8$ respectively.

These results are not unexpected. The delayed neutron generation terms, in the two-group diffusion equations (2.3.1) and (2.3.2), containing $\chi^1_{2,8}$ and $\chi^2_{1,8}$ respectively, are the largest and smallest generation terms. The observation that $dP/d\alpha_1$ and $dP/d\alpha_2$ are essentially the same as $dP/d\alpha_7$ and $dP/d\alpha_8$ respectively, results from the fact that the delayed neutron generation terms containing α_1 and α_2 are essentially the same as those containing α_7 and α_8 respectively. In other words, the sensitivity derivatives, $dR/d\alpha_i$, have the same ranking as the corresponding delayed neutron generation terms containing α_i.

The magnitudes of the delayed neutron generation terms will change with burnup as the relative amounts of U-238 and Pu-239 change. During a year's operation of the reactor modelled in this study, the U-238 inventory decreases by 1.3% while the Pu-239 inventory increases by 12.5% [12]. This will change the relative magnitudes of the delayed neutron generation terms, and correspondingly, the relative magnitudes

of the sensitivity derivatives, resulting in a re-distribution of the rankings of the sensitivity derivatives.

Corresponding pairs of sensitivity derivatives occur in a fixed ratio, i.e.,

$$\frac{dP}{d\alpha_1} \Big/ \frac{dP}{d\alpha_2} = \frac{dP}{d\alpha_3} \Big/ \frac{dP}{d\alpha_4} = \frac{dP}{d\alpha_5} \Big/ \frac{dP}{d\alpha_6} = \frac{dP}{d\alpha_7} \Big/ \frac{dP}{d\alpha_8} .$$

For the particular problem being studied here, the ratio has a value of 1.35. The reason why, for example, $dP/d\alpha_1$ and $dP/d\alpha_2$ is referred to as a corresponding pair is that they are related through the constraint that $\alpha_1 + \alpha_2 = 1$. The fixed ratio is independent of time and rod ejection time.

The fixed ratio between pairs of derivatives may be explained by re-examining the theoretical development. The adjoint solutions, $\underline{\Phi}$, are independent of the parameter $\underline{\alpha}$, i.e., the adjoint operator $\underline{\underline{L}}^*$ and the right-hand sides of the adjoint equations are independent of the particular parameter under study. In this case, $\underline{\Phi}$ is simply a weight function. The analytical expression, equation (2.3.43), for $dR/d\alpha_i$ contains S_1^i and S_2^i, and $\underline{\psi}$ which is dependent on α_i. These quantities have already been defined.

Consider the corresponding pair of parameters α_1 and α_2. Then,

for α_1, $S_1^i = S_1^1 \neq 0$ and $S_2^i = S_2^1 = 0$, and

for α_2, $S_1^i = S_1^2 = 0$ and $S_2^i = S_2^2 \neq 0$.

(Refer to table 2.3.1 for the analytical expressions for S_1^i and S_2^i.)

Now, re-examine the system of equations (2.3.31), $\underline{\underline{L}}\ \underline{\psi} = \underline{S}^i$. Again, consider the corresponding pair α_1 and α_2. Then

$$\underline{\underline{L}}\ \underline{\psi} = \begin{bmatrix} S_1^1 \\ 0 \\ 0 \\ 0 \\ 0 \\ 0 \end{bmatrix} \quad \text{for } \alpha_1, \text{ and} \tag{5.3.2}$$

$$\underline{\underline{L}}\ \underline{\psi} = \begin{bmatrix} 0 \\ S_2^2 \\ 0 \\ 0 \\ 0 \\ 0 \end{bmatrix} \quad \text{for } \alpha_2 \ . \tag{5.3.3}$$

The solution, $\underline{\psi}$, is directly proportional to $\underline{S}^i$. Also, $dR/d\alpha_1$ is directly proportional to both $\underline{S}^i$ and $\underline{\psi}$. Also, the ratio of $dR/d\alpha_1$ to $dR/d\alpha_2$ dependent upon the ratio of S_1^1 to S_2^2. For the particular problem being studied here, the ratio $S_1^1/S_2^2 = 1$. The situation is identical for all other corresponding pairs of parameters, and since

$$\frac{S_1^1}{S_2^2} = \frac{S_1^3}{S_2^4} = \frac{S_1^5}{S_2^6} = \frac{S_1^7}{S_2^8} = 1 \ ,$$

all corresponding pairs of sensitivity derivatives should occur in a fixed ratio (as is observed).

More formally,

$$\frac{dR}{d\alpha_i} = \langle \underline{\Phi}, \underline{S}^i \rangle + \hat{P}\ [\underline{\Phi}, \underline{\psi}] \ , \tag{2.3.43}$$

or writing this out for α_1 and α_2, the sensitivity derivatives are

$$\frac{dR}{d\alpha_1} = \left\langle \underline{\Phi}, \begin{bmatrix} S_1^1 \\ 0 \\ 0 \\ 0 \\ 0 \\ 0 \end{bmatrix} \right\rangle + \hat{P} \left\{ \underline{\Phi}, \underline{\underline{L}}^{-1} \begin{bmatrix} S_1^1 \\ 0 \\ 0 \\ 0 \\ 0 \\ 0 \end{bmatrix} \right\}, \text{ and} \tag{5.3.4}$$

$$\frac{dR}{d\alpha_2} = \left\langle \underline{\Phi}, \begin{bmatrix} 0 \\ S_2^2 \\ 0 \\ 0 \\ 0 \\ 0 \end{bmatrix} \right\rangle + \hat{P} \left\{ \underline{\Phi}, \underline{\underline{L}}^{-1} \begin{bmatrix} 0 \\ S_2^2 \\ 0 \\ 0 \\ 0 \\ 0 \end{bmatrix} \right\}, \tag{5.3.5}$$

where $\underline{\underline{L}}^{-1}$ is the inverse of the operator $\underline{\underline{L}}$. From equations (5.3.4) and (5.3.5) it can be seen that the ratio of $dR/d\alpha_1$ to $dR/d\alpha_2$ only depends on the relative values of S_1^1 and S_2^2. Since the relative values of all other corresponding values of S are the same, all other corresponding pairs of sensitivity derivatives will be in the same ratio as $dR/d\alpha_1$ and $dR/d\alpha_2$.

Another interesting observation is made by examining the values of the sensitivity derivatives, at some time $\bar{t}$, relative to the smallest derivatives at that time $\bar{t}$. These relative values are tabulated in table 5.3.7. These relative values are essentially independent of time. The variations are at most only 2% with one notable exception. The sensitivity derivatives with respect to α_3 and α_4, at $\bar{t}$ = 45 seconds, are 16% higher than what they were at $\bar{t}$ = 10 seconds, though the ratio of $dP/d\alpha_3$ to $dP/d\alpha_4$ still remains at the fixed value of 1.35. No explanation could be found for this behaviour.

This behaviour is unfortunate because if the relative values of the sensitivity derivaties were completely time independent, (the 2% variation noted above would not be considered a strong time dependence) this would eliminate the need for re-solving the adjoint equations and re-calculating the sensitivity derivatives each time the responce is changed. All that would need to be done is to re-normalise the sensitivity derivatives each time the responce is changed.

(b) Power Density Responce

All the observations and explanations for the behaviour of the power sensitivity derivatives hold true for the power density sensitivity derivatives. This is not unexpected. The only part of the calculation of the sensitivity derivatives that is dependent upon the type of responce being studied is the solution of the adjoint equations. The real dependence is in the weight functions, $f(r,t)$ and $g(r,t)$, of the responce functionals, since these functions form the right-hand side of the adjoint system of equations. Further, the adjoint solutions are really only dependent on the relative value of the weight functions. Referring to equations (5.1.2), (5.1.3), (5.1.5), and (5.1.6), it is observed that the relative value of the weight functions is the same for both the power and power density responces, i.e.,

$$\frac{f(r,t)}{g(r,t)} = \frac{\Sigma_f^1}{\Sigma_f^2} \quad .$$

Table 5.3.7 Relative values of the Sensitivity Derivatives (The "relative values" are relative to the smallest sensitivity derivative at each value of $\bar{t}$).

α_i	$\bar{t} = 10$	$\bar{t} = 15$	$\bar{t} = 20$	$\bar{t} = 25$	$\bar{t} = 30$	$\bar{t} = 45$
α_1	1.35	1.35	1.35	1.35	1.35	1.35
α_2	1.00	1.00	1.00	1.00	1.00	1.00
α_3	1.64	1.68	1.72	1.76	1.80	1.91
α_4	1.22	1.25	1.28	1.31	1.34	1.42
α_5	2.97	2.96	2.95	2.95	2.94	2.93
α_6	2.20	2.19	2.19	2.19	2.18	2.17
α_7	1.36	1.37	1.38	1.38	1.38	1.39
α_8	1.01	1.01	1.02	1.03	1.03	1.03

Note: $\bar{t}$ has units of seconds.

In light of this, it can be seen that as long as responce functionals of the form of those in equations (5.1.1) and (5.1.4) are used, there is no need to solve the adjoint problem all over again for the power density responce. All that needs to be done is to re-normalise the sensitivity derivatives obtained during the calculation of the power sensitivity derivatives.

The power density sensitivity derivatives, $dPD/d\alpha_i$, are presented in tables 5.3.8 to 5.3.13. The tables are set up in exactly the same manner as tables 5.3.1 to 5.3.6 with one exception. The power density responces are evaluated at the phase-space coordinates $(\bar{r},\bar{t})$ where $\bar{r}$ is the radial coordinate, in the reactor, where the peak power density occurs. The value of $\bar{r}$ (in metres) is also indicated in the tables. The power density sensitivity derivatives have units of kilowatts per litre (KW/ℓ). The power density sensitivity derivatives were evaluated at the same times, $\bar{t}$, as the power sensitivity derivatives.

5.3.3 Sensitivity Calculations

In this section, the results of the sensitivity calculations are presented. The sensitivity derivatives were used to predict the responces resulting from changes in the parameter vector. These responces are referred to as the "predicted perturbed responces". To verify these predictions, the responces were calculated by solving the forward transient equations. These responces are referred to as the "recalculated responces".

Table 5.3.8 Power Density Sensitivity Derivatives, $dPD/d\alpha_i$, for a Rod Ejection Time of 2 Seconds (Normalised to $\Delta\underline{\alpha}_1$)

α_i	$\bar{\underline{t}} = 10$ $\bar{r} = 0.2244$	$\bar{\underline{t}} = 15$ $\bar{r} = 0.2244$	$\bar{\underline{t}} = 20$ $\bar{r} = 0.2244$	$\bar{\underline{t}} = 25$ $\bar{r} = 0.2244$
α_1	57.3	170.9	491.9	1308.4
α_2	42.5	126.9	365.1	971.2
α_3	69.6	212.8	628.1	1712.7
α_4	51.7	158.2	466.9	1273.1
α_5	126.2	375.5	1078.6	2863.1
α_6	93.7	278.7	800.6	2125.2
α_7	57.8	173.5	502.6	1344.9
α_8	43.0	129.0	373.5	999.6

Table 5.3.9 Power Density Sensitivity Derivatives, $dPD/d\alpha_i$, for a Rod Ejection Time of 2 Seconds (Normalised to $\Delta\underline{\alpha}_5$)

α_i	$\bar{\underline{t}} = 10$ $\bar{r} = 0.2244$	$\bar{\underline{t}} = 15$ $\bar{r} = 0.2244$	$\bar{\underline{t}} = 20$ $\bar{r} = 0.2244$	$\bar{\underline{t}} = 25$ $\bar{r} = 0.2244$
α_1	98.3	307.9	945.3	2682.6
α_2	73.0	228.6	701.7	1991.3
α_3	119.4	383.4	1207.0	3511.4
α_4	88.7	285.0	897.2	2610.1
α_5	216.5	676.6	2072.8	5870.0
α_6	160.7	502.3	1538.6	4357.1
α_7	99.2	312.7	965.8	2757.4
α_8	73.8	232.4	717.8	2049.5

Note: $\bar{\underline{t}}$ has units of seconds.
$\bar{r}$ has units of metres.
$dPD/d\alpha_i$ has units of kW/ℓ.

Table 5.3.10 Power Density Sensitivity Derivatives, $dPD/d\alpha_i$, for a Rod Ejection Time of 10 Seconds (Normalised to $\Delta\alpha_1$)

α_i	$\frac{\bar{t}}{r} = 10$ / 0.2244	$\frac{\bar{t}}{r} = 15$ / 0.2244	$\frac{\bar{t}}{r} = 20$ / 0.2244	$\frac{\bar{t}}{r} = 30$ / 0.2244
α_1	17.9	60.6	184.2	1354.9
α_2	13.3	45.0	136.8	1005.7
α_3	21.8	75.5	235.2	1815.1
α_4	16.2	56.2	174.8	1349.2
α_5	39.4	133.1	404.0	2958.5
α_6	29.3	98.8	299.9	2196.1
α_7	18.0	61.2	187.1	1392.5
α_8	13.4	45.5	139.1	1035.0

Table 5.3.11 Power Density Sensitivity Derivatives, $dPD/d\alpha_i$, for a Rod Ejection Time of 10 Seconds (Normalised to $\Delta\alpha_5$)

α_i	$\frac{\bar{t}}{r} = 10$ / 0.2244	$\frac{\bar{t}}{r} = 15$ / 0.2244	$\frac{\bar{t}}{r} = 20$ / 0.2244	$\frac{\bar{t}}{r} = 30$ / 0.2244
α_1	19.7	102.2	320.1	2844.2
α_2	14.6	75.9	237.6	2111.2
α_3	24.0	127.5	408.7	3810.3
α_4	17.8	94.8	303.8	2832.3
α_5	43.3	224.6	702.0	6210.8
α_6	32.2	166.7	521.1	4610.3
α_7	19.8	103.2	325.1	2923.2
α_8	14.7	76.7	241.6	2172.7

Note: $\frac{\bar{t}}{r}$ has units of seconds.
$dPD/d\alpha_i$ has units of kW/ℓ.

Table 5.3.12 Power Density Sensitivity Derivatives, $dPD/d\alpha_i$, for a Rod Ejection Time of 30 Seconds (Normalised to $\Delta\alpha_1$)

α_i	$\bar{t}$ = 10 $\bar{r}$ = 0.3686	$\bar{t}$ = 20 $\bar{r}$ = 0.3686	$\bar{t}$ = 30 $\bar{r}$ = 0.2244	$\bar{t}$ = 45 $\bar{r}$ = 0.2244
α_1	5.02	17.8	105.6	2030.6
α_2	3.72	13.2	78.4	1507.3
α_3	6.12	22.6	139.9	2875.2
α_4	4.55	16.8	104.0	2137.2
α_5	11.0	39.0	230.7	4411.2
α_6	8.19	28.9	171.3	3274.4
α_7	5.02	17.9	106.8	2091.1
α_8	3.73	13.3	79.4	1554.2

Table 5.3.13 Power Density Sensitivity Derivatives, $dPD/d\alpha_i$, for a Rod Ejection Time of 30 Seconds (Normalised to $\Delta\alpha_5$)

α_i	$\bar{t}$ = 10 $\bar{r}$ = 0.3686	$\bar{t}$ = 20 $\bar{r}$ = 0.3686	$\bar{t}$ = 30 $\bar{r}$ = 0.2244	$\bar{t}$ = 45 $\bar{r}$ = 0.2244
α_1	5.90	20.9	181.1	4664.9
α_2	4.38	15.6	134.4	3462.8
α_3	7.20	26.6	240.0	6605.2
α_4	5.35	19.8	178.4	4909.8
α_5	13.0	45.9	395.8	10133.7
α_6	9.63	34.1	293.8	7522.1
α_7	5.90	21.0	183.3	4803.9
α_8	4.39	15.6	136.2	3570.5

Note: $\bar{t}$ has units of seconds.
$\bar{r}$ has units of metres.
$dPD/d\alpha_i$ has units of kW/ℓ.

The results of the power sensitivity calculations are presented in tables 5.3.14 to 5.3.16. The tables contain predicted and recalculated changes in the responce as well as the responce for each parameter vector. The times, $\bar{t}$, at which the responces are evaluated, as well as the parameter vectors used, are indicated in the first two columns of the tables. Some results are shown graphically in figure 5.3.2.

The perturbations in the parameter vectors may be thought of as uncertainites in the vectors so that the resulting perturbations in the responces are the uncertainties in the responces due to uncertainties in the parameter vectors. From the results in tables 5.3.14 to 5.3.16, a table of uncertainties in the predicted responces, table 5.3.17, was constructed for the parameter vectors $\underline{\alpha}_1$, $\underline{\alpha}_2$, $\underline{\alpha}_3$, and $\underline{\alpha}_4$. The parameter vectors are shown in the first column of the table. The second column contains the fractional perturbations (or uncertainties) in the fast components of the unperturbed parameter vector. Columns 3 to 6 contain the predicted perturbations (uncertainites) in the power responce at given times $\bar{t}$ during the transient.

From table 5.3.17, it can be seen that the uncertainty in the responce increases with increasing time during a transient. Further, the shorter the rod ejection time, the larger the uncertainty in the power. For example, an uncertainty of only 2.4% in the fast components of the parameter vector results in a 6.1% uncertainty in the predicted reactor power level after 25 seconds into the transient for a rod ejection time of 2 seconds. A 7.2% uncertainty in the fast components of the parameter vector results in an uncertainty of 18.4% in the reactor power

Table 5.3.14 Power Responce for a Rod Ejection Time of 2 Seconds

$\bar{t}$(sec)	$\underline{\alpha}_i$	Predicted Perturbed Responce		Recalculated Responce	
		ΔP(MWt)	P(MWt)	ΔP(MWt)	P(MWt)
10	$\underline{\alpha}_0$	0.0	247.1	0.0	247.1
	$\underline{\alpha}_1$	6.3	253.4	6.3	253.4
	$\underline{\alpha}_2$	-6.3	240.8	-6.1	241.0
	$\underline{\alpha}_3$	12.6	259.7	12.8	259.9
	$\underline{\alpha}_4$	18.9	266.0	19.4	266.5
	$\underline{\alpha}_5$	1.9	249.0	1.9	249.0
	$\underline{\alpha}_6$	3.8	250.9	3.9	251.0
15	$\underline{\alpha}_0$	0.0	542.7	0.0	542.7
	$\underline{\alpha}_1$	20.1	562.8	20.1	562.8
	$\underline{\alpha}_2$	-20.1	522.6	-19.4	523.3
	$\underline{\alpha}_3$	40.2	582.9	41.0	583.7
	$\underline{\alpha}_4$	60.3	603.0	62.6	605.3
	$\underline{\alpha}_5$	6.3	549.0	6.3	549.0
	$\underline{\alpha}_6$	12.6	555.3	12.7	555.4
20	$\underline{\alpha}_0$	0.0	1171.7	0.0	1171.7
	$\underline{\alpha}_1$	57.5	1229.2	57.5	1229.2
	$\underline{\alpha}_2$	-57.5	1114.2	-54.8	1116.9
	$\underline{\alpha}_3$	115.0	1286.7	117.8	1289.5
	$\underline{\alpha}_4$	172.5	1344.2	181.1	1352.8
	$\underline{\alpha}_5$	18.3	1190.0	18.3	1190.0
	$\underline{\alpha}_6$	36.6	1208.3	36.9	1208.6
25	$\underline{\alpha}_0$	0.0	2519.0	0.0	2519.0
	$\underline{\alpha}_1$	154.4	2673.4	154.4	2673.4
	$\underline{\alpha}_2$	-154.4	2364.6	-145.5	2373.5
	$\underline{\alpha}_3$	308.8	2827.8	318.3	2837.3
	$\underline{\alpha}_4$	463.2	2982.2	492.3	3011.3
	$\underline{\alpha}_5$	49.6	2568.6	49.6	2568.6
	$\underline{\alpha}_6$	99.2	2618.2	100.3	2619.3

Table 5.3.15 Power Responce for a Rod Ejection Time of 10 Seconds

$\bar{t}$(sec)	α_i	Predicted Perturbed Responce		Reclaculated Responce	
		ΔP(MWt)	P(MWt)	ΔP(MWt)	P(MWt)
10	α_0	0.0	99.0	0.0	99.0
	α_1	1.9	100.9	1.9	100.9
	α_2	-1.9	97.1	-1.9	97.1
	α_3	3.8	102.8	3.9	102.9
	α_4	5.7	104.7	5.9	104.9
	α_5	0.5	99.5	0.5	99.5
	α_6	1.0	100.0	1.0	100.0
15	α_0	0.0	238.0	0.0	238.3
	α_1	7.1	245.4	7.1	245.4
	α_2	-7.1	231.2	-6.9	231.4
	α_3	14.2	252.5	14.4	252.7
	α_4	21.3	259.6	21.9	260.2
	α_5	2.0	240.3	2.0	240.3
	α_6	4.0	242.3	4.1	242.4
20	α_0	0.0	525.6	0.0	525.6
	α_1	21.7	547.3	21.7	547.3
	α_2	-21.7	503.9	-20.8	504.8
	α_3	43.4	569.0	44.3	569.9
	α_4	65.1	590.7	67.8	593.4
	α_5	6.5	532.1	6.5	532.1
	α_6	13.0	538.6	13.2	538.8
30	α_0	0.0	2443.0	0.0	2443.0
	α_1	160.0	2603.0	160.0	2603.0
	α_2	-160.0	2283.0	-150.0	2293.0
	α_3	320.0	2763.0	330.7	2773.7
	α_4	480.0	2923.0	512.8	2955.8
	α_5	50.2	2493.2	50.2	2493.2
	α_6	100.4	2543.4	101.5	2544.5

Table 5.3.16 Power Responce for a Rod Ejection Time of 30 Seconds

$\bar{t}$(sec)	$\alpha_{\bar{i}}$	Predicted Perturbed Responce		Recalculated Responce	
		ΔP(MWt)	P(MWt)	ΔP(MWt)	P(MWt)
10	$\alpha_{\bar{1}0}$	0.0	37.1	0.0	37.1
	$\alpha_{\bar{1}1}$	0.5	37.6	0.5	37.6
	$\alpha_{\bar{1}2}$	-0.5	36.6	-0.6	36.5
	$\alpha_{\bar{1}3}$	1.0	38.2	1.2	38.3
	$\alpha_{\bar{1}4}$	1.5	38.6	1.8	38.9
	$\alpha_{\bar{1}5}$	0.1	37.2	0.1	37.2
	$\alpha_{\bar{1}6}$	0.2	37.3	0.2	37.3
20	$\alpha_{\bar{1}0}$	0.0	74.0	0.0	74.0
	$\alpha_{\bar{1}1}$	2.0	76.0	2.0	76.0
	$\alpha_{\bar{1}2}$	-2.0	72.0	-1.9	72.1
	$\alpha_{\bar{1}3}$	4.0	78.0	4.1	78.1
	$\alpha_{\bar{1}4}$	6.0	80.0	6.2	80.2
	$\alpha_{\bar{1}5}$	0.5	74.5	0.5	74.5
	$\alpha_{\bar{1}6}$	1.0	75.0	1.0	75.0
30	$\alpha_{\bar{1}0}$	0.0	293.2	0.0	293.2
	$\alpha_{\bar{1}1}$	12.7	305.9	12.7	305.9
	$\alpha_{\bar{1}2}$	-12.7	280.5	-12.2	281.0
	$\alpha_{\bar{1}3}$	25.4	318.6	26.1	319.3
	$\alpha_{\bar{1}4}$	38.1	331.3	40.1	333.3
	$\alpha_{\bar{1}5}$	3.5	296.7	3.5	296.7
	$\alpha_{\bar{1}6}$	7.0	300.2	7.1	300.3
45	$\alpha_{\bar{1}0}$	0.0	3064.8	0.0	3064.8
	$\alpha_{\bar{1}1}$	243.1	3307.9	243.1	3307.9
	$\alpha_{\bar{1}2}$	-243.1	2821.7	-224.6	2840.2
	$\alpha_{\bar{1}3}$	486.2	3551.0	506.2	3571.0
	$\alpha_{\bar{1}4}$	729.3	3794.1	791.1	3855.9
	$\alpha_{\bar{1}5}$	73.3	3138.1	73.3	3138.1
	$\alpha_{\bar{1}6}$	146.6	3211.4	148.5	3213.3

Table 5.3.17 Uncertainties in Power Responce for Given Changes in the Parameter Vector

Rod Ejection Time of 2 Seconds

$\underline{\alpha}_i$	CIFC	$\bar{t}$=10 sec	$\bar{t}$=15 sec	$\bar{t}$=20 sec	$\bar{t}$=25 sec
$\underline{\alpha}_1$	+2.4%	2.5%	3.7%	4.9%	6.1%
$\underline{\alpha}_2$	-2.4	-2.5	-3.7	-4.9	-6.1
$\underline{\alpha}_3$	+4.8	5.1	7.4	9.8	12.3
$\underline{\alpha}_4$	+7.2	7.6	11.1	14.7	18.4

Rod Ejection Time of 10 Seconds

$\underline{\alpha}_i$	CIFC	$\bar{t}$=10 sec	$\bar{t}$=15 sec	$\bar{t}$=20 sec	$\bar{t}$=30 sec
$\underline{\alpha}_1$	+2.4%	1.9%	3.0%	4.1%	6.5%
$\underline{\alpha}_2$	-2.4	-1.9	-3.0	-4.1	-6.5
$\underline{\alpha}_3$	+4.8	3.8	6.0	8.3	13.1
$\underline{\alpha}_4$	+7.2	5.8	8.9	12.4	19.6

Rod Ejection Time of 30 Seconds

$\underline{\alpha}_i$	CIFC	$\bar{t}$=10 sec	$\bar{t}$=20 sec	$\bar{t}$=30 sec	$\bar{t}$=45 sec
$\underline{\alpha}_1$	+2.4%	1.3%	2.7%	4.3%	7.9%
$\underline{\alpha}_2$	-2.4	-1.3	-2.7	-4.3	-7.9
$\underline{\alpha}_3$	+4.8	3.0	5.4	8.7	15.9
$\underline{\alpha}_4$	+7.2	4.0	8.1	13.0	23.8

NOTE: CIFC ≡ Change In Fast Components

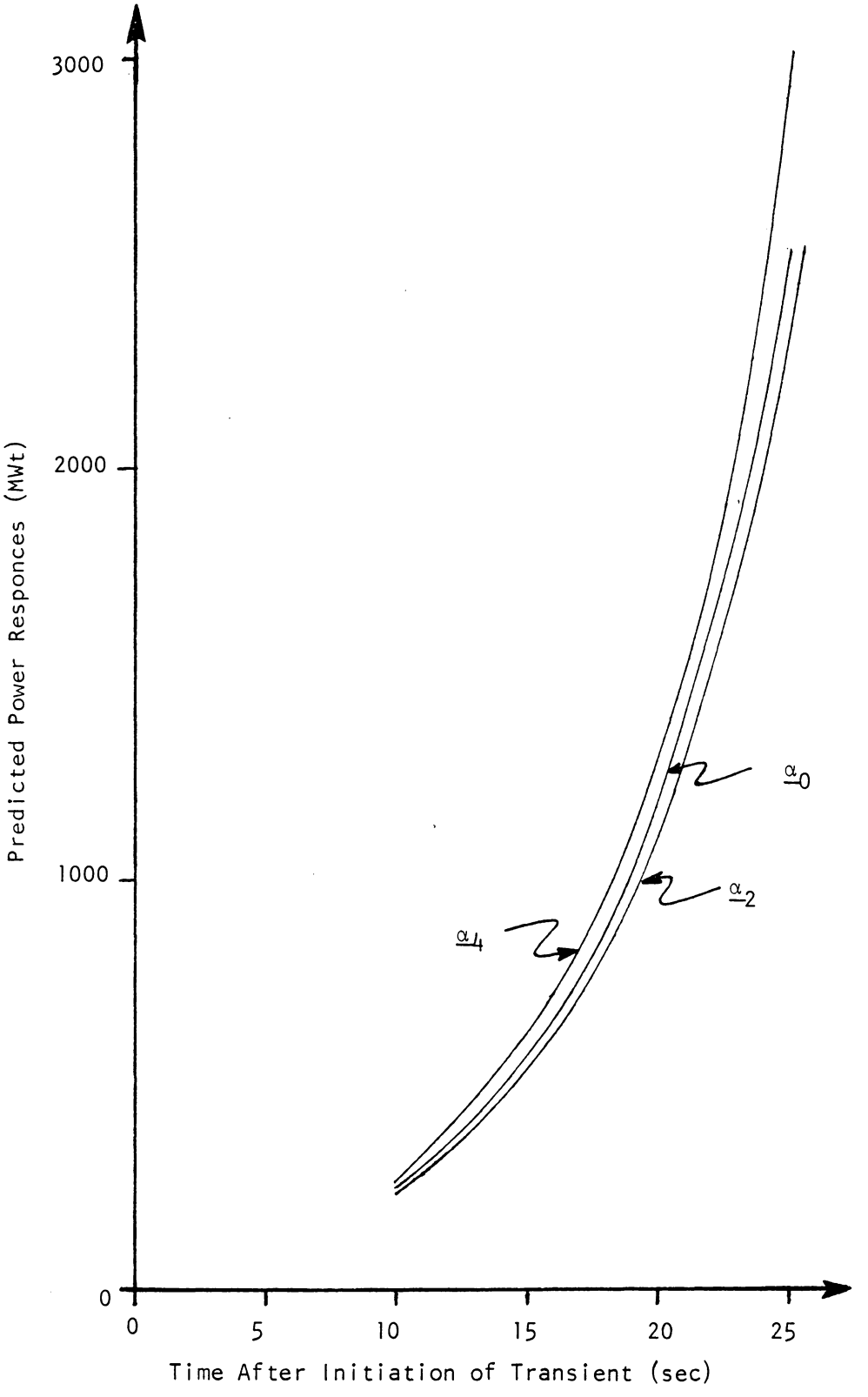

Fig. 5.3.2 Predicted Power Responces for a Rod Ejection Time of 2 Seconds for the Parameter Vectors $\underline{\alpha}_0$, $\underline{\alpha}_2$ and $\underline{\alpha}_4$.

level after 25 seconds into the transient for a rod ejection time of 2 seconds. Even for the slowest transient (rod ejection time of 30 seconds), the uncertainties are quite large. For example, 45 seconds into the transient, an uncertainty of 7.2% in the fast components of the parameter vector results in a 23.8% uncertainty in the predicted power level.

In comparing the predicted power responces with the recalculated ones, the largest discrepancy is only 1.6%. This occurs for the 30-second rod ejection time transient at $\bar{t}$ = 45 seconds for the perturbed parameter vector $\underline{\alpha}_4$. The predicted power level is 3794 MWt whereas the recalculated power level is 3856 MWt. In most other cases, the discrepancy is less than 1%. From these results it can be concluded that the predicted responces are amply verified by the recalculated responces.

The results of the power density calculations are presented in tables 5.3.18 to 5.3.20. These tables are set up in exactly the same manner as tables 5.3.14 to 5.3.16 for the power calculations. The radial location, $\bar{r}$, at which the power density peaks is indicated in the first column of the tables. The power density responces are evaluated using the same perturbed parameters $\underline{\alpha}_i$, times, $\bar{t}$, into the transient, and rod ejection times as for the power responces. The uncertainties in the predicted power density responces are tabulated in table 5.3.21. This table is set up in exactly the same manner as table 5.3.17.

The behaviour of the uncertainties in the power density responces is exactly the same as the behaviour of the power responces. They increase with time during a transient and increase as the rod ejection

Table 5.3.18 Power Density Responce for a Rod Ejection Time of 2 Seconds

$\bar{t}$(sec)		Predicted Perturbed Responce		Recalculated Responce	
$\bar{r}$(m)	α_i	ΔPD(kW/ℓ)	PD(kW/ℓ)	ΔPD(kW/ℓ)	PD(kW/ℓ)
10	α_0	0.0	59.6	0.0	59.6
0.2244	α_1	1.6	61.2	1.6	61.2
	α_2	-1.6	58.0	-1.4	58.2
	α_3	3.2	62.8	3.1	62.7
	α_4	4.8	64.4	4.7	64.3
	α_5	0.5	60.1	0.5	60.1
	α_6	1.0	60.6	1.0	60.6
15	α_0	0.0	131.0	0.0	131.0
0.2244	α_1	4.8	135.8	4.8	135.8
	α_2	-4.8	126.2	-4.7	126.3
	α_3	9.6	140.6	9.9	140.9
	α_4	14.4	145.4	15.1	146.1
	α_5	1.5	132.5	1.5	132.5
	α_6	3.0	134.0	3.0	134.0
20	α_0	0.0	282.8	0.8	282.8
0.2244	α_1	13.9	296.7	13.9	296.7
	α_2	-13.9	268.9	-13.2	269.6
	α_3	27.8	310.6	28.4	311.2
	α_4	41.7	324.5	43.7	326.5
	α_5	4.4	287.2	4.4	287.2
	α_6	8.8	291.6	8.9	291.7
25	α_0	0.0	608.0	0.0	608.0
0.2244	α_1	37.2	645.2	37.2	645.2
	α_2	-37.2	570.8	-35.1	572.9
	α_3	74.4	682.4	76.8	684.8
	α_4	111.6	719.6	118.8	726.8
	α_5	11.9	619.9	11.9	619.9
	α_6	23.8	631.8	24.2	632.2

Table 5.3.19 Power Density Responce for a Rod Ejection Time of 10 Seconds

$\bar{t}$(sec) $\bar{r}$(m)	α_i	Predicted Perturbed Responce		Recalculated Responce	
		ΔPD(kW/ℓ)	PD(kW/ℓ)	ΔPD(kW/ℓ)	PD(kW/ℓ)
10	α_0	0.0	23.9	0.0	23.9
0.2244	α_1	0.5	24.4	0.5	24.4
	α_2	-0.5	23.4	-0.5	23.4
	α_3	1.0	24.9	0.9	24.8
	α_4	1.5	25.4	1.4	25.3
	α_5	0.1	24.0	0.1	24.0
	α_6	0.2	24.1	0.2	24.1
15	α_0	0.0	57.5	0.0	57.5
0.2244	α_1	1.7	59.2	1.7	59.2
	α_2	-1.7	55.8	-1.7	55.8
	α_3	3.4	60.9	3.5	61.0
	α_4	5.1	62.6	5.3	62.8
	α_5	0.5	58.0	0.5	58.0
	α_6	1.0	58.5	1.0	58.5
20	α_0	0.0	126.9	0.0	126.9
0.2244	α_1	5.2	132.1	5.2	132.1
	α_2	-5.2	121.7	-5.1	121.8
	α_3	10.4	137.3	10.6	137.5
	α_4	15.6	142.5	16.3	143.2
	α_5	1.5	128.4	1.5	128.4
	α_6	3.0	129.9	3.1	130.0
30	α_0	0.0	589.6	0.0	589.6
0.2244	α_1	38.7	628.3	38.7	628.3
	α_2	-38.7	550.9	-36.2	553.4
	α_3	77.4	667.0	79.8	669.4
	α_4	116.1	705.7	123.8	713.4
	α_5	12.1	601.7	12.1	601.7
	α_6	24.2	613.8	24.5	614.1

Table 5.3.20 Power Density Responce for a Rod Ejection Time of 30 Seconds

$\bar{t}$(sec) $\bar{r}$(m)	$\underline{\alpha}_i$	Predicted Perturbed Responce		Recalculated Responce	
		ΔPD(kW/ℓ)	PD(kW/ℓ)	ΔPD(kW/ℓ)	PD(kW/ℓ)
10	$\underline{\alpha}_0$	0.0	8.71	0.0	8.71
0.3686	$\underline{\alpha}_1$	0.14	8.85	0.14	8.85
	$\underline{\alpha}_2$	-0.14	8.57	-0.14	8.57
	$\underline{\alpha}_3$	0.28	8.99	0.28	8.99
	$\underline{\alpha}_4$	0.42	9.13	0.42	9.13
	$\underline{\alpha}_5$	0.03	8.74	0.03	8.74
	$\underline{\alpha}_6$	0.06	8.77	0.06	8.77
20	$\underline{\alpha}_0$	0.0	17.6	0.0	17.6
0.3686	$\underline{\alpha}_1$	0.5	18.1	0.5	18.1
	$\underline{\alpha}_2$	-0.5	17.1	-0.5	17.1
	$\underline{\alpha}_3$	1.0	18.6	1.0	18.6
	$\underline{\alpha}_4$	1.5	19.1	1.4	19.0
	$\underline{\alpha}_5$	0.1	17.7	0.1	17.7
	$\underline{\alpha}_6$	0.2	17.8	0.2	17.8
30	$\underline{\alpha}_0$	0.0	70.8	0.0	70.8
0.2244	$\underline{\alpha}_1$	3.0	73.8	3.0	73.8
	$\underline{\alpha}_2$	-3.0	67.8	-3.0	67.8
	$\underline{\alpha}_3$	6.0	76.8	6.3	77.1
	$\underline{\alpha}_4$	9.0	79.8	9.6	80.4
	$\underline{\alpha}_5$	0.8	71.6	0.8	71.6
	$\underline{\alpha}_6$	1.6	72.4	1.7	72.5
45	$\underline{\alpha}_0$	0.0	739.7	0.0	739.7
0.2244	$\underline{\alpha}_1$	58.7	798.4	58.7	798.4
	$\underline{\alpha}_2$	-58.7	681.0	-54.2	685.5
	$\underline{\alpha}_3$	117.4	857.1	122.2	861.9
	$\underline{\alpha}_4$	176.1	915.8	190.9	930.6
	$\underline{\alpha}_5$	17.7	757.4	17.7	757.4
	$\underline{\alpha}_6$	35.4	775.1	35.8	775.5

Table 5.3.21 Uncertainties in Power Density Responce for Given Changes in the Parameter Vector

Rod Ejection Time of 2 Seconds

$\underline{\alpha}_i$	CIFC	$\bar{t}$=10 sec	$\bar{t}$=15 sec	$\bar{t}$=20 sec	$\bar{t}$=25 sec
$\underline{\alpha}_1$	+2.4%	2.7%	3.7%	4.9%	6.1%
$\underline{\alpha}_2$	-2.4	-2.7	-3.7	-4.9	-6.1
$\underline{\alpha}_3$	+4.8	5.4	7.3	9.8	12.2
$\underline{\alpha}_4$	+7.2	8.1	11.0	14.7	18.4

Rod Ejection Time of 10 Seconds

$\underline{\alpha}_i$	CIFC	$\bar{t}$=10 sec	$\bar{t}$=15 sec	$\bar{t}$=20 sec	$\bar{t}$=30 sec
$\underline{\alpha}_1$	+2.4%	2.1%	3.0%	4.1%	6.6%
$\underline{\alpha}_2$	-2.4	-2.1	-3.0	-4.1	-6.6
$\underline{\alpha}_3$	+4.8	4.2	5.9	8.2	13.1
$\underline{\alpha}_4$	+7.2	6.3	8.9	12.3	19.7

Rod Ejection Time of 30 Seconds

$\underline{\alpha}_i$	CIFC	$\bar{t}$=10 sec	$\bar{t}$=20 sec	$\bar{t}$=30 sec	$\bar{t}$=45 sec
$\underline{\alpha}_1$	+2.4%	1.6%	2.8%	4.2%	7.9%
$\underline{\alpha}_2$	-2.4	-1.6	-2.8	-4.2	-7.9
$\underline{\alpha}_3$	+4.8	3.2	5.7	8.5	15.9
$\underline{\alpha}_4$	+7.2	4.8	8.5	12.7	23.8

NOTE: CIFC ≡ Change In Fast Components

time decreases. Again, for the most rapid transient (2-second rod ejection time) a 2.4% uncertainty in the fast components of the parameter vector results in a 6.1% uncertainty in the power density while a 7.2% uncertainty in the fast components results in an 18.4% uncertainty in the power density, both at 25 seconds into the transient. The largest uncertainty in power density, for the cases studied, was 23.8% at 45 seconds into the 30-second rod ejection time transient. This was due to a 7.2% uncertainty in the fast components of the parameter vector.

As for the power responces, the largest discrepancy between the predicted and recalculated power density responces is 1.6%. This occurs for the 30-second rod ejection time transient at $\bar{t} = 45$ seconds for the perturbed parameter vector $\underline{\alpha}_4$. In most other cases, the discrepancy is less than 1%. Again, the recalculated responces amply verify the predicted perturbed responces.

The results of the sensitivity calculations may have important safety implications. It has been shown that uncertainties of upto 7.2% in the delayed neutron spectra can lead to uncertainties of over 18.4% in the reactor responces. It is questionable as to whether or not such large uncertainties are acceptable. Every effort should be made to reduce these uncertainties. Further, if either the number of delayed neutron groups or the number of energy groups is increased, the uncertainties in the parameter vector will be larger than in the cases studied in this work and the corresponding uncertainties in the power and power density will be amplified.

5.4 Computational Effort

While computational efficiency was not a major concern when performing the calculations in this work, some mention is made of the computational effort required to perform the sensitivity analysis. Also, suggestions as to how to fully take advantage of Cacuci's sensitivity methodology to reduce computational effort are made.

A sensitivity analysis performed by perturbing the parameters in the forward (kinetics) equations requires repeated solution of the full system of equations. The number of times the system must be solved equals the product of the number of parameter vectors and the number of transients to be studied. In this work, seven parameter vectors were used and three transients were studied, hence, the forward equations had to be solved 21 times. It can be seen how this could become a prohibitively tedious and expensive exercise. For example, to solve the forward equations (2.3.1) to (2.3.6), using 31 spatial mesh points, time steps of one second, and a total of 100 time steps, requires 77 seconds of central processing unit (CPU) time on an IBM-3032 processor.

To perform a sensitivty analysis applying Cacuci's methodology, which was the basis of this work, the adjoint system of equations (2.2.13) must be solved each time the responce is changed. If a large number of responces are to be studied, this could be as tedious and as expensive as performing the sensitivity analysis by repeatedly solving the forward equations. In this work, a total of 24 responces were studied, i.e., 8 responces for each of 3 transients. To solve the adjoint equations (2.2.13) using the same spatial and time meshes as for

the forward equations requires 80 seconds of CPU time. It is not difficult to see that this is an inefficient way of performing a sensitivity analysis. By closely examining equation (2.2.13), it is easy to see how the need for solving the adjoint equations so many times can be drastically reduced.

The adjoint operator $\underline{\underline{L}}^*$ does not change, i.e., it is evaluated using the unperturbed parameter vector $\underline{\alpha}_0$ whereas the forward operator $\underline{\underline{L}}$ changes each time the parameter vector is perturbed. Now suppose that a particular transient is being studied. For each responce, the adjoint source term, $\underline{\$}^*$, of equation (2.2.13) changes. Instead of repeatedly solving equation (2.2.13) for each $\underline{\$}^*$, the source term can be written as a matrix, rather than a vector, where the columns in the matrix are the adjoint sources corresponding to each responce. Hence, the adjoint solutions, corresponding to each responce, may be found by solving equation (2.2.13) only once! This is a tremendous reduction in computational effort since each time the adjoint equations are solved, the coefficient matrix has to be inverted at each time step. Repeatedly solving the adjoint equations for each of the 8 responces for a given transient, and using 100 time steps, would require a total of 800 inversions of the coefficient matrix. Using the more efficient method just described, only 100 inversions would be required. Hence, it is seen how Cacuci's generalised methodology lends itself to high computational efficiency as compared with repeated solution of the forward equations for performing a sensitivity analysis.

Chapter 6

Conclusions and Recommendations

6.1 Summary

An analysis to study the sensitivity of the power and power density to the uncertainties in the delayed neutron spectra for an LMFBR was performed. A set of sensitivity derivatives was derived for the power and power density during three transients in which the central control rod is ejected over times of 2, 10, and 30 seconds. The generalised sensitivity methodology developed by Cacuci et al [10] was applied to the time dependent multigroup diffusion equations in order to derive the sensitivity derivatives. The multigroup equations are linear. Two linear responces, total core power and power density, were studied.

6.2 Conclusions

It was shown that the power and power density were sensitive to uncertainties in the delayed neutron spectra. For the particular model studied, the power and power density were found to be most sensitive to uncertainties in $\chi^{1}_{2,8}$, i.e., the spectrum of delayed neutron precursor group 2, resulting from the fission of U-238, producing delayed neutrons in energy group 1, while the responces were found to be least sensitive to uncertainties in $\chi^{2}_{1,8}$.

The power and power density were found to be more sensitive to uncertainties in the delayed neutron spectra during rapid transients than during slower transients. Thus, for a given point $(\overline{r}, \overline{t})$ in the

phase-space, the more rapid the transient, the larger the uncertainty in the power and power density at that point.

Small uncertainties in the delayed neutron spectra resulted in large uncertainties in the power and power density. For example, for a rod ejection accident in which the rod is fully ejected in 2 seconds, a 2.4% uncertainty in the fast components of the delayed neutron spectra results in a 6.1% uncertainty in the predicted power and power density, whereas a 7.2% uncertainty in the fast components results in an 18.4% uncertainty in the repsonces.

The predicted responces were verified by recalculating them by repeated solution of the forward equations. The largest discrepancy between predicted and recalculated responces was 1.6%.

The versatility of Cacuci's sensitivy methodology has been demonstrated. In particular, it has been shown not only to be accurate, but also to be computationally more efficient than repeated solution of the forward equations. It is the concept of the Fréchet derivative that makes Cacuci's methodology particularly versatile. The Fréchet differentiation of the governing equations, which may be linear or nonlinear, results in a system of linear differential equations. Hence, the existence of the adjoint system of equations, upon which the methodology is based, is guaranteed. The methodology is equally applicable to linear and nonlinear problems, though the Fréchet differentiation of the nonlinear problem may be more difficult to perform than for the linear case.

6.3 Recommendations

The results of the sensitivity analysis indicate the need for improving the accuracy of delayed neutron spectra data. The component that needs the most attention is $\chi^1_{2,8}$. Recall that this quantity is an integral quantity, i.e., the second precursor group on the model used contains the 2, 0.5, and 0.2 second half-life precursor groups, and energy group 1 ranges from 10^7 MeV down to 0.11 MeV. Detailed spectral measurements in these precursor groups for U-238 should be done. The second most important parameter is $\chi^2_{2,8}$. However, it is perhaps more important to improve upon the spectral data for the third most important parameter $\chi^1_{1,9}$ than for $\chi^2_{2,8}$. The sensitivity derivatives derived in this study were calculated using the fuel isotopic concentrations for a new core. As the fuel burnup increases, the Pu-239 concentration will increase due to breeding, and so the sensitivity of the responces to uncertainties in $\chi^1_{1,9}$ will increase. The sensitivity analysis should be coupled with a burnup analysis to study this.

The present model may easily be modified to study the effects of uncertainties in other parameters in the reactor kinetics equations. For instance, the effects of uncertainties in the delayed neutron fractions should be studied. Saphier and Yiftah [25] have shown that for "a hypothetical abrupt control rod withdrawal, equivalent to \$0.3 of reactivity at the left outer region of the (LMFBR) core", an uncertainty of 5% in the effective delayed neutron fraction resulted in an uncertainty of 20% in the resulting power transient 6 seconds after its initiation. As well as transient analysis, the delayed neutron fra-

ctions are important in predicting reactivity worths of the fuel, sodium voids, and control rods [26]. Improved delayed neutron fraction data is still being sought [26].

The model could be refined by using two spatial dimensions instead of one. With such a model, a sensitivity analysis for quantities such as the linear power density and linear heat rate (power added to coolant per unit axial length) could be performed. Functionals for these quantities can be written in the form of equation (2.2.7).

The number of energy and precursor groups could be increased so as to perform a more detailed sensitivity analysis. However, this would greatly increase the computational effort involved.

REFERENCES

1. Maffre, J., "Nuclear: Some Forward Motion", Nuclear Industry, Vol. 28, No. 11, Nov. 1981.

2. "The World List of Nuclear Power Plants", Nuclear News, Vol. 25, No. 2, Feb. 1982.

3. Graham, J., Fast Reactor Safety, Academic Press, N.Y., 1971.

4. Hetrick, D. L., Dynamics of Nuclear Reactors, The University of Chicago Press, Chicago, 1971.

5. Saphier, D., D. Ilberg, and S. Yiftah, "Sensitivity of LMFBR Calculations to Basic Data Sources", ANS Topical Meeting, Atlanta (1974).

6. Reeder, P. L. and R. A. Warner, "Average Energy of Delayed Neutrons from Individual Precursors and Estimation of Equilibrium Spectra", Nuc. Sci. and Eng., 79, 56-64 (1981).

7. Embrechts, M. J., "Two-Dimensional Cross-Section Sensitivity and Uncertainty Analysis for Fusion Reactor Blankets", Ph.D. Dissertation, VPI and SU, Blacksburg, Virginia (1981).

8. Oblow, E. M., Nuc. Sci. and Eng., 59, 187-189 (1976); and Corrigendum, Nuc. Sci. and Eng., 65, 428 (1978).

9. Dubie, D. and D. Dudziak, "Higher-Order Terms in Sensitivity Analysis Via a Differential Approach", Los Alamos National Laboratory, University of California, Los Alamos. (Rough Draft; Undated)

10. Cacuci, D. G., C. F. Weber, E. M. Oblow, and J. H. Marable, "Sensitivity Theory for General Systems of Nonlinear Equations", Nuc. Sci. and Eng., 75, 88-110 (1980).

11. Tomović, R., Sensitivity Analysis of Dynamic Systems, McGraw-Hill Electronic Sciences Series, McGraw-Hill Book Company, Inc., N.Y., 1963.

12. Chang, Y. I. and C. E. Till, "INFCE/5 Fast Breeder Reactor Studies: Design and Performance Characteristics of Alternative Fuels and Fuel Cycles", INFCE/5-TM-3, Argonne National Laboratory, July 1978.

13. Lewins, J., Nuclear Reactor Kinetics and Control, University College, London, England, Pergamon Press, 1978.

14. Onega, R. J., An Introduction to Fission Reactor Theory, University Publications, Blacksburg, Virginia, 1975.

15. Milton, L. J. and R. E. Prael, "A User's Manual for the Monte Carlo Code VIM", FRA Technical Memorandum No. 84, Applied Physics Division, ANL, Feb. 1976.

16. ENDF/B-IV, National Nuclear Data Center, Brookhaven National Laboratory.

17. Reactor Physics Constants, ANL-5800, 2nd Ed., Argonne National Laboratory, July 1963.

18. Keepin, G. R., Physics of Nuclear Kinetics, Addison-Wesley Publishing Company, Inc., Reading, Mass., 1965.

19. Clinch River Breeder Reactor Plant, Preliminary Safety Analysis Report, Vol. 4, Project Management Corporation.

20. International Mathematical and Statistics Libraries, Inc., Vol. 1, 8th Ed., Houston, Texas, July 1980.

21. Duderstadt, J. J. and L. J. Hamilton, Nuclear Reactor Analysis, John Wiley and Sons, Inc., N. Y., 1976.

22. Thomas, J. R., "Reactor Statics Module, RS-8, Three-Group Criticality Program", Report on NSF Grant GZ-2888, Aug. 1974.

23. International Mathematical and Statistics Libraries, Inc., Vol. 2, 8th Ed., Houston, Texas, July 1980.

24. Roper, D. L., The Dirac Delta Function in Physics with Applications, Physical Biological Sciences Misc., 1972.

25. Saphier, D. and S. Yiftah, "Sensitivity of LMFBR Kinetic Parameters and Transient Calculations to Uncertainties in the Higher Plutonium Cross Sections", Trans. Am. Nuc. Soc., Vol. 19, pp 392-393, Oct. 1974.

26. Fischer, E. A., "Integral Measurements of the Effective Delayed Neutron Fractions in the Fast Critical Assembly SNEAK", Nuc. Sci. and Eng., 62, 105-116 (1977).

27. Finlayson, B. A., The Method of Weighted Residuals and Variational Principles With Application in Fluid Mechanics, Heat and Mass Transfer, Academic Press, New York, 1972.

Appendix 1

FRÉCHET DIFFERENTIATION OF FORWARD EQUATIONS

A. Definition of Fréchet Derivative

The following definition of the Fréchet derivative was taken from Finlayson [27].

In order to be able to perform the sensitivity analysis, it is necessary to take the Fréchet derivative of the governing (forward) equations (2.2.1). To illustrate how this is done, consider the homogeneous differential equation

$$N(u) = 0 \ , \tag{A.1.1}$$

where N may be a linear or nonlinear operator. The derivative of the operator equation (A.1.1) in the direction ϕ is defined by

$$N_u' \phi \equiv \lim_{\varepsilon \to 0} \frac{N(u+\varepsilon\phi) - N(u)}{\varepsilon} = \left[\frac{\partial}{\partial \varepsilon} N(u+\varepsilon\phi) \right]_{\varepsilon=0} \ . \tag{A.1.2}$$

The Fréchet differential of the operator in the direction ϕ is $N_u'\phi$ and the Fréchet derivative of the operator is N_u', where the subscript u in N_u' means that the operator is differentiated with respect to the argument "u".

B. Fréchet Derivative of the Forward Equations

The system of forward equations (2.3.1) to (2.3.6) is a linear homogeneous system. The equations may be written in the form

$$L[X(\alpha);\ \alpha] = 0\ , \tag{A.1.3}$$

where

$\alpha \equiv$ a parameter which appears explicitly in the equations,

$X(\alpha) \equiv$ the state variable which is implicitly dependent upon α, and

$L \equiv$ the linear operator operating on X.

The state vector X may also be dependent upon space and time, but the space and time variables have been suppressed from the argument list of X since they do not enter into the analysis that follows.

To take the Fréchet derivative of equation (A.1.3) with respect to the parameter "α", the definition (A.1.2) is applied directly to equation (A.1.3) giving

$$0 = L'_{\alpha}\,\delta\alpha \equiv \lim_{\varepsilon\to 0} \frac{L[X(\alpha+\varepsilon\delta\alpha);\ \alpha+\varepsilon\delta\alpha] - L[X(\alpha);\ \alpha]}{\varepsilon}$$

$$= \left\{ \frac{\partial}{\partial\varepsilon} L\ [X(\alpha + \varepsilon\delta\alpha);\ \alpha + \varepsilon\delta\alpha] \right\}_{\varepsilon=0}$$

$$= \left\{ \frac{\partial}{\partial\varepsilon} L\ [X(\alpha) + \varepsilon\delta\alpha\frac{\partial X}{\partial\alpha}\ ;\ \alpha + \varepsilon\delta\alpha] \right\}_{\varepsilon=0} \quad \text{(higher order terms vanish as } \varepsilon\to 0\text{)}$$

$$= \left\{ \frac{\partial}{\partial\varepsilon} L\ [X(\alpha);\ \alpha + \varepsilon\delta\alpha] \right\}_{\varepsilon=0} + \left\{ \frac{\partial}{\partial\varepsilon} L\ [\varepsilon\delta\alpha\ \frac{\partial X}{\partial\alpha}\ ;\ \alpha + \varepsilon\delta\alpha] \right\}_{\varepsilon=0}$$

$$= \left\{ \frac{\partial}{\partial \varepsilon} L\ [X(\alpha);\ \alpha + \varepsilon\delta\alpha] \right\}_{\varepsilon=0} + \left\{ L[\ \frac{\partial}{\partial \varepsilon}\ (\varepsilon\delta\alpha\ \frac{\partial X}{\partial \alpha}\ );\ \alpha + \varepsilon\delta\alpha] \right\}_{\varepsilon=0}$$

$$= \left\{ \frac{\partial}{\partial \varepsilon} L\ [X(\alpha);\ \alpha + \varepsilon\delta\alpha] \right\}_{\varepsilon=0} + L\ [\frac{\partial X}{\partial \alpha}\ ;\ \alpha]\ \delta\alpha$$

$$= \left\{ \frac{\partial}{\partial \varepsilon} L\ [X(\alpha);\ \alpha + \varepsilon\delta\alpha] \right\}_{\varepsilon=0} + L[\psi(\alpha);\ \alpha]\ \delta\alpha$$

$$= \quad ① \quad + \quad ② \quad , \qquad \text{(A.1.4)}$$

where $\psi(\alpha) = \partial X/\partial\alpha$.

Consider a linear homogeneous differential equation of the form of the diffusion equation. For example, consider

$$L[X(\alpha);\ \alpha] = \nabla^2 X + \frac{\partial X}{\partial t} + \alpha X = 0\ , \qquad \text{(A.1.5)}$$

where the linear operator L is

$$L \equiv \nabla^2 + \frac{\partial}{\partial t} + \alpha\ . \qquad \text{(A.1.6)}$$

Applying the definition of the Fréchet derivative, the following results are obtained:

$$① \equiv \left\{ \frac{\partial}{\partial \varepsilon}\ [\nabla^2 X + \frac{\partial X}{\partial t} + (\alpha + \varepsilon\delta\alpha)X] \right\}_{\varepsilon=0}$$

$$= \left\{ \frac{\partial}{\partial \varepsilon} \left[\nabla^2 X + \frac{\partial X}{\partial t} + \alpha X + \varepsilon \delta\alpha X \right] \right\}_{\varepsilon=0}$$

$$= X\delta\alpha \text{ , and}$$

$$\textcircled{2} \equiv L[\psi(\alpha);\ \alpha]\ \delta\alpha$$

$$= \left[\nabla^2\psi + \frac{\partial\psi}{\partial t} + \alpha\psi\right]\ \delta\alpha.$$

Then,

$$0 = \textcircled{1} + \textcircled{2}$$

$$= \left[\nabla^2\psi + \frac{\partial\psi}{\partial t} + \alpha\psi + X\right]\ \delta\alpha$$

$$= L_\alpha'\ \delta\alpha \text{ ,}$$

where

$$L_\alpha' = \nabla^2\psi + \frac{\partial\psi}{\partial t} + \alpha\psi + X = 0 \qquad \text{(A.1.7)}$$

is the Fréchet derivative of equation (A.1.5) with respect to the parameter "α".

Since α is a real variable, it can be shown that the Fréchet derivative of equation (A.1.5) is identical to the derivative of equation (A.1.5) with respect to "α" in the ordinary sense, i.e.,

$$0 = \frac{d}{d\alpha}\left[\nabla^2 X + \frac{\partial X}{\partial t} + \alpha X\right]$$

$$= \nabla^2\psi + \frac{\partial\psi}{\partial t} + \alpha\psi + X$$

$$= L'_{\alpha} .$$

Hence, to find the Fréchet derivatives of the forward equations (2.3.1) to (2.3.6) with respect to the parameter "α", the equations need only be differentiated with respect to "α" in the ordinary sense of differentiation.

Appendix 2

DERIVATION OF ADJOINT OPERATOR, BILINEAR CONCOMITANT, AND ADJOINT BOUNDARY CONDITIONS

A. Introduction

The forward equations (2.3.1) to (2.3.6) can be written in operator notation as

$$\underline{\underline{L}}\ \underline{X}\ (r,\ t;\ \underline{\alpha}) = 0\ . \tag{A.2.1}$$

It will be implicit throughout the following analyses that all notation used has been previously defined in the main body of the text.

When the system of equations (A.2.1) is differentiated, in the Fréchet sense, with respect to "$\underline{\alpha}$", the following system results:

$$\underline{\underline{L}}\ \underline{\psi}\ (r,\ t;\ \underline{\alpha}) = \underline{S}^{i}\ (r,\ t;\ \underline{\alpha})\ . \tag{A.2.2}$$

To derive expressions for the sensitivity derivatives, it is necessary to find the system of equations that is adjoint to the system (A.2.2). In so doing, it is necessary to define the operator $\underline{\underline{L}}^{*}$, that is adjoint to $\underline{\underline{L}}$, by

$$\langle \underline{\underline{L}}^{*}\ \underline{\Phi},\ \underline{\psi} \rangle = \langle \underline{\Phi},\ \underline{\underline{L}}\ \underline{\psi} \rangle + P[\underline{\Phi},\ \underline{\psi}]\ . \tag{A.2.3}$$

To find the adjoint of $\underline{\underline{L}}$, it is necessary to find the adjoint of each element of $\underline{\underline{L}}$, and then transponse the resultant operator. Most of the elements of $\underline{\underline{L}}$ contain additive constants which are self-adjoint. However, some elements contain the differential operators

$$\nabla_r^2 \equiv \frac{1}{r}\frac{\partial}{\partial r}\left(r\frac{\partial}{\partial r}\right) , \qquad (A.2.4)$$

and

$$-\frac{\partial}{\partial t} . \qquad (A.2.5)$$

The first operator is the radial term of the Laplacian in cylindrical gemoetry which appears in the multigroup diffusion equations, and the second operator is the time derivative that appears in the precursor equations.

B. Adjoint of ∇_r^2

Using equation (A.2.3), the following analysis will yield the adjoint of ∇_r^2, the bilinear concomitant, and the adjoint boundary conditions. Now,

$$\langle \Phi, \nabla_r^2 \psi \rangle = \int_0^{t_f} \int_0^R \Phi \frac{1}{r}\frac{\partial}{\partial r}\left(r\frac{\partial \psi}{\partial r}\right) r\,dr\, 2\pi H dt .$$

For convenience, the notation $\int_0^{t_f} 2\pi H dt$ will be dropped since it does not enter explicitly into the following analysis, but its presence remains implicit. Then,

$$\langle \Phi, \nabla_r^2 \psi \rangle = \int_0^R \Phi \frac{1}{r}\frac{\partial \psi}{\partial r}\left(r\frac{\partial \psi}{\partial r}\right) r\,dr$$

$$= \left[\Phi\, r\frac{\partial \psi}{\partial r}\right]_0^R - \int_0^R \frac{\partial \psi}{\partial r}\left(r\frac{\partial \Phi}{\partial r}\right) dr$$

$$= \left[\Phi \; r \frac{\partial \psi}{\partial r} - \psi \; r \frac{\partial \Phi}{\partial r} \right]_0^R + \int_0^R \psi \; \frac{1}{r} \frac{\partial}{\partial r} \left(r \frac{\partial \Phi}{\partial r} \right) \; r dr$$

$$= \left[\Phi \; r \frac{\partial \psi}{\partial r} - \psi \; r \frac{\partial \Phi}{\partial r} \right]_0^R + \langle \nabla_r^2 \; \Phi, \; \psi \rangle \quad . \tag{A.2.6}$$

Putting this in the form of equation (A.2.3),

$$\langle \nabla_r^2 \; \Phi, \; \psi \rangle = \langle \Phi, \; \nabla_r^2 \; \psi \rangle + P[\Phi, \; \psi] \; , \tag{A.2.7}$$

where

$$P[\Phi,\psi] = - \left[\Phi \; r \frac{\partial \psi}{\partial r} - \psi \; r \frac{\partial \Phi}{\partial r} \right]_0^R \tag{A.2.8}$$

is the bilinear concomitant. In trying to make the bilinear concomitant vanish, using the boundary conditions of the forward equations, the boundary conditions for the adjoint equations can be found. Since $\partial\psi/\partial r\Big|_{r=0} = 0$ and $\psi(R) = 0$ (symmetry and boundary conditions for forward equations), to make the bilinear concomitant vanish, the conditions $\partial\Phi/\partial r\Big|_{r=0} = 0$ and $\Phi\ (R) = 0$ are imposed.

In summary, the following results were obtained from the above analysis:

(1) ∇_r^2 is self-adjoint ,

(2) $\frac{\partial \Phi}{\partial r}\Big|_{r=0} = 0$ (symmetry condition), and

(3) $\Phi\ (R) = 0$ (boundary condition).

C. Adjoint of $-\partial/\partial t$

Consider the inner product

$$\langle \Phi, -\frac{\partial \psi}{\partial t} \rangle = \int_0^R \int_0^{t_f} \Phi(-\frac{\partial \psi}{\partial t})\, dt\, 2\pi H r dr \ .$$

For convenience, the notation $\int_0^R 2\pi H r dr$ will be dropped since it does not enter explicitly into the following analysis, but its presence remains implicit. Then,

$$\langle \Phi, -\frac{\partial \psi}{\partial t} \rangle = \int_0^{t_f} \Phi(-\frac{\partial \psi}{\partial t})\, dt$$

$$= \left[-\Phi\psi\right]_0^{t_f} + \int_0^{t_f} \psi \frac{\partial \Phi}{\partial t}\, dt$$

$$= [\Phi(0)\psi(0) - \Phi(t_f)\psi(t_f)] + \int_0^{t_f} \psi \frac{\partial \Phi}{\partial t}\, dt \ . \qquad \text{(A.2.9)}$$

Putting this in the form of equation (A.2.3),

$$\langle \frac{\partial \Phi}{\partial t}, \psi \rangle = \langle \Phi, -\frac{\partial \psi}{\partial t} \rangle + P[\Phi, \psi] \ , \qquad \text{(A.2.10)}$$

where

$$P[\Phi, \psi] = [\Phi(t_f)\psi(t_f) - \Phi(0)\psi(0)] \qquad \text{(A.2.11)}$$

is the bilinear concomitant. Recall from section 2.2.4 that the adjoint boundary conditions are obtained by requiring that all terms in $P[\Phi, \psi]$ that contain unknown values of ψ must vanish. Since $\psi(t_f)$ is the only

unknown, the term $\Phi(t_f)\ \psi(t_f)$ must vanish by requiring $\Phi(t_f)$ to vanish, reducing equation (A.2.11) to

$$\hat{P}[\Phi,\ \psi] = -\ \Phi(0)\psi(0)\ . \tag{A.2.12}$$

Recall that the spatial integration was implicit, so equation (A.2.12) should be written as

$$\hat{P}[\Phi,\psi] = -\ 2\pi H \int_0^R \Phi(r,0)\psi(r,0)rdr\ . \tag{A.2.13}$$

Since there are four precursors, the bilinear concomitant will contain four terms, one for each precursor, i.e.,

$$\begin{aligned}\hat{P}[\Phi,\ \psi] = &-\ 2\pi H \int_0^R \Phi^3(r,0)\psi^3(r,0)\ rdr \\ &-\ 2\pi H \int_0^R \Phi^4(r,0)\psi^4(r,0)rdr \\ &-\ 2\pi H \int_0^R \Phi^5(r,0)\psi^5(r,0)rdr \\ &-\ 2\pi H \int_0^R \Phi^6(r,0)\psi^6(r,0)rdr\ ,\end{aligned} \tag{A.2.14}$$

where the notation used has been defined in the text.

In summary, the following results were obtained from the above analysis:

(1) $-\frac{\partial}{\partial t}^{*} = \frac{\partial}{\partial t}$, and

(2) $\Phi(t_f) = 0$ (final condition) .

Appendix 3

NUMBER DENSITIES OF ISOTOPES USED IN VIM CALCULATION

Isotope	Number Densities[a]			
	MOX Fuel	Blanket	Clad	Coolant
Pu-240	.61192-3[b]			
Pu-241	.32252-3			
U-235	.36169-4	.44593-4		
U-238	.17800-1	.22251-1		
Pu-239	.21465-2			
Pu-238	.31558-4			
Pu-242	.76709-4			
O-16	.42050-1	.44593-1		
Cr			.13950-1	
Ni			.69770-2	
Fe			.50380-1	
Na-23				.22791-1

[a]Units of atoms/barn-cm

[b].61192-3 ≡ .61192 x 10^{-3}

Appendix 4

DIFFUSION DATA FOR THREE-REGION REACTOR

Central Control Region

Group	D	Σ_a	$\nu\Sigma_f^*$	$\Sigma_s^{1/2}$	Σ_p	$\nu\Sigma_{f8}$	$\nu\Sigma_{f9}$	B_z^2
1	4.9866	0.0	0.0	9.3671-3	-	0.0	0.0	9.5612-4
2	3.3354	0.0	0.0	0.0	-	0.0	0.0	9.5612-4

Mixed Oxide Core Region

Group	D	Σ_a	$\nu\Sigma_f^*$	$\Sigma_s^{1/2}$	Σ_p	$\nu\Sigma_{f8}$	$\nu\Sigma_{f9}$	B_z^2
1	1.4126	4.5948-3	1.6722-3	7.8710-3	0.1-2	2.1913-3	5.4823-3	9.5612-4
2	1.0020	8.8918-3	1.9362-3	0.0	0.1-2	1.3427-6	6.3527-3	9.5612-4

Depleted Uranium Blanket Region

Group	D	Σ_a	$\nu\Sigma_f^*$	$\Sigma_s^{1/2}$	Σ_p	$\nu\Sigma_{f8}$	$\nu\Sigma_{f9}$	B_z^2
1	1.1410	3.2328-3	1.0040-4	1.0524-2	0.0	3.5202-3	0.0	9.5612-4
2	0.8451	8.1697-3	2.8022-4	0.0	0.0	2.4884-6	0.0	9.5612-4

NOTES:
1. All symbols have been defined in text.
2. Diffusion coefficients have units of cm.
   Macroscopic cross sections have units of cm^{-1}.
   Transverse bucklings have units of cm^{-2}
4. Σ_p = 0.1-1 for both groups in central control region when reactor is critical.

Appendix 5

DELAYED NEUTRON FRACTIONS AND DECAY CONSTANTS

A. Delayed Neutron Fractions

Tabulations, by Keepin [18], for prompt and delayed neutron yields from fast fission were used to calculate delayed neutron fractions. The six precursor groups were collapsed into two groups. The first three precursor groups were collapsed into "group 1" and the second three groups were collapsed into "group 2". Delayed neutron fractions for U-238 and Pu-239 were calculated by

$$\text{Delayed Neutron Fraction } (\beta) = \frac{\text{Absolute Group Yield (\%)}}{100 \times \text{Prompt Neutron Yield } (\bar{\nu})} .$$

(1) U-238

$$\beta_1^8 = \frac{1.285}{100 \times 2.79} = 0.0046$$

$$\beta_2^8 = \frac{2.835}{100 \times 2.79} = 0.0102$$

$$\beta^8 = \beta_1^8 + \beta_2^8 = 0.0148$$

Note: All notation used has been defined in the text.

(2) Pu - 239

$$\beta_1^9 = \frac{0.336}{100 \times 3.09} = 0.0011$$

$$\beta_2^9 = \frac{0.294}{100 \times 3.09} = 0.0010$$

$$\beta^9 = \beta_1^8 + \beta_2^8 = 0.0021$$

(3) Effective Delayed Neutron Fraction

The delayed neutron fractions for U-238 and Pu-239 were weighted by the relative power fractions of the two isotopes. The power fractions were taken from the VIM calculation for the MOX core.

$$\beta_{eff} = (0.0148)\ (0.1247) + (0.0021)\ (0.6718)$$

$$= 0.00326$$

B. Precursor Group Decay Constants

Decay constants for precursors from fast fission were taken from Keepin [18]. As for the delayed neutron fractions, the six precursor groups were collapsed into two groups.

(1) U-238

$$\frac{\beta_1^8}{\lambda_1^8} = \sum_{i=1}^{3} \frac{\beta_i^8}{\lambda_i^8} = 0.0948 = \frac{0.0048}{\lambda_1^8}$$

$$\frac{\beta_2^8}{\lambda_2^8} = \sum_{i=4}^{6} \frac{\beta_i^8}{\lambda_i^8} = 0.0186 = \frac{0.0102}{\lambda_2^8}$$

From these, the following decay constants and half lives are obtained:

$$\lambda_1^8 = 0.0485 \text{ sec}^{-1} \qquad T_{1/2} = 14.3 \text{ sec}$$

$$\lambda_2^8 = 0.5484 \text{ sec}^{-1} \qquad T_{1/2} = 1.26 \text{ sec}$$

(2) Pu-239

Using the same procedure as above, the following results are obtained:

$$\lambda_1^9 = 0.0398 \text{ sec}^{-1} \qquad T_{1/2} = 17.4 \text{ sec}$$

$$\lambda_2^9 = 0.4519 \text{ sec}^{-1} \qquad T_{1/2} = 1.53 \text{ sec}$$

Appendix 6

FINITE DIFFERENCE SCHEMES

A. Radial Component of Laplacian in Cylindrical Geometry

The radial component of the Laplacian appears in the multigroup diffusion equations. In cylindrical geometry, the radial component of the Laplacian of the function $\phi(r,t)$ is

$$\nabla_r^2 \phi = \frac{1}{r} \frac{\partial}{\partial r} \left(r \frac{\partial \phi}{\partial r} \right)$$

$$= \frac{\partial^2 \phi}{\partial r^2} + \frac{1}{r} \frac{\partial \phi}{\partial r} \, . \qquad \text{(A.6.1)}$$

At the origin ($r = 0$), L'Hospital's rule must be applied to the second term in equation (A.6.1) giving

$$\nabla_r^2 \phi \Big|_{r=0} = 2 \frac{\partial^2 \phi}{\partial r^2} \Big|_{r=0} \, . \qquad \text{(A.6.2)}$$

(a) Difference Approximation for r > 0

Consider the following mesh scheme for the radial direction:

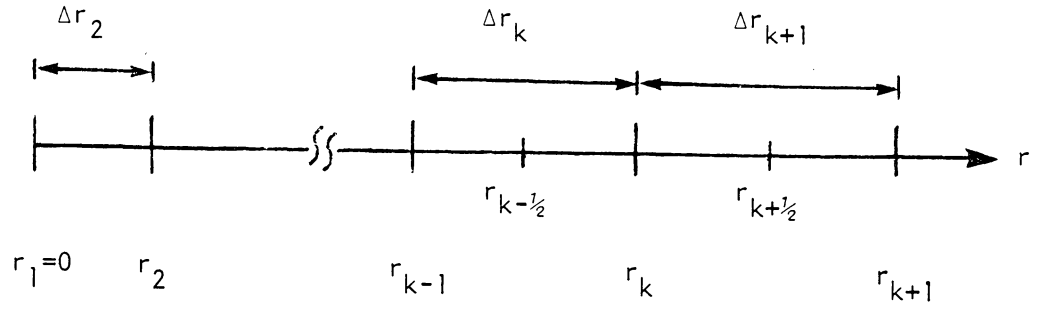

The first derivative of ϕ, at $r = r_k$, is approximated by the central difference formula

$$\left.\frac{\partial \phi}{\partial r}\right|_{r_k} \cong \frac{\phi_{k+1} - \phi_{k-1}}{\Delta r_k + \Delta r_{k+1}} = d_k \quad . \tag{A.6.3}$$

The second derivative of ϕ is approximated by

$$\left.\frac{\partial^2 \phi}{\partial r^2}\right|_{r_k} = \left.\frac{\partial d}{\partial r}\right|_{r_k} \cong \frac{d_{k+\frac{1}{2}} - d_{k-\frac{1}{2}}}{\frac{1}{2}(\Delta r_k + \Delta r_{k+1})}$$

$$\cong \frac{\dfrac{\phi_{k+1} - \phi_k}{\Delta r_{k+1}} - \dfrac{\phi_k - \phi_{k-1}}{\Delta r_k}}{\frac{1}{2}(\Delta r_k + \Delta r_{k+1})} \quad . \tag{A.6.4}$$

Combining equations (A.6.3) and (A.6.4), equation (A.6.1) for the radial component of the Laplacian is approximated by

$$\left.\nabla_r^2 \phi\right|_{r_k} \cong \left[\frac{2}{(\Delta r_k + \Delta r_{k+1})\Delta r_k} - \frac{1}{r_k(\Delta r_k + \Delta r_{k+1})}\right]\phi_{k-1}$$

$$-\left[\frac{2}{\Delta r_k \, \Delta r_{k+1}}\right]\phi_k$$

$$+\left[\frac{2}{(\Delta r_k + \Delta r_{k+1})\Delta r_{k+1}} + \frac{1}{r_k(\Delta r_k + \Delta r_{k+1})}\right]\phi_{k+1} \quad . \tag{A.6.5}$$

(b) Difference Approximation at r = 0

Using a central difference approximation and applying the symmetry condition at r = 0, equation (A.6.2) is approximated by

$$\nabla_r^2 \phi \Big|_{r=0} \cong \frac{4(\phi_2 - \phi_1)}{(\Delta r_2)^2} . \qquad \text{(A.6.6)}$$

B. First Order Time Derivative

First order time derivatives appear in the differential equations governing the concentrations of the precursors. The first order derivative of the function $\phi(r,t)$, evaluated at time $t = t_n$, is approximated by the forward difference formulation

$$\frac{\partial \phi}{\partial t} \Big|_{t_n} \cong \frac{\phi_{n+1} - \phi_n}{t_{n+1} - t_n} . \qquad \text{(A.6.7)}$$

The vita has been removed from the scanned document

SAFETY IMPLICATIONS OF A SENSITIVITY ANALYSIS OF THE REACTOR KINETICS PARAMETERS FOR FAST BREEDER REACTORS

by

Robert Joseph Florian

ABSTRACT

The delayed neutron spectra for LMFBRs are not as well known as those for LWRs. These spectra are necessary for kinetics calculations which play an important role in safety and accident analyses. In this study, a sensitivity analysis was performed to study the sensitivity of the reactor power and power density to uncertainties in the delayed neutron spectra during a rod ejection accident.

The generalised methodology, developed by Cacuci et. al., was used to derive a set of sensitivity derivatives. This method is based on the use of adjoints so that it is not necessary to repeatedly solve the governing (kinetics) equations to obtain the sensitivity derivatives. This is of particular importance when large systems of equations are used.

A two-energy multigroup and two precursor group model was formulated for the INFCE reference design MOX-fuelled LMFBR. The accidents studied were central control rod ejections with ejection times of 2, 10, and 30 seconds.

The power and power density responces were found to be most sensitive to uncertainties in the spectrum of the second delayed neutron precursor group, resulting from the fission of U-238, producing neutrons in the first energy group. It was found, for example, that for a rod ejection time of 30 seconds, an uncertainty of 7.2% in the fast components of the spectra resulted in a 24% uncertainty in the predicted power and power density. These responces were recalculated by repeatedly solving the kinetics equations. The maximum discrepancy was only 1.6%.

The versatility and accuracy of Cacuci's methodology has been demonstrated. The results of the sensitivity analysis indicates the need for improved delayed neutron spectral data in order to reduce the uncertainties in the accident analyses.

The model can be extended by using more energy groups, more precursor groups, and more spatial dimensions. Other important responces that may be studied are the linear power density, linear heat rate, and reactivity worths.